MODEL TEST OF A TURBO-TYPE ENERGY ABSORBER FOR AIRCRAFT CARRIER ARRESTING GEAR

Thomas Albert Morgenfeld

NAVAL POSTGRADUATE SCHOOL
Monterey, California

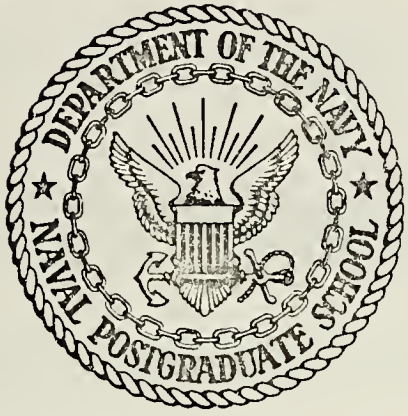

THESIS

MODEL TEST OF A TURBO-TYPE ENERGY ABSORBER
FOR
AIRCRAFT CARRIER ARRESTING GEAR

by

Thomas Albert Morgenfeld

Thesis Advisor: M. H. Vavra

March 1973

Approved for public release; distribution unlimited.

Model Test of a Turbo-Type Energy Absorber for Aircraft Carrier Arresting Gear

by

Thomas Albert Morgenfeld
Lieutenant, United States Navy
B.S., United States Naval Academy, 1965

Submitted in partial fulfillment of the
requirements for the degree of

MASTER OF SCIENCE IN AERONAUTICAL ENGINEERING

from the

NAVAL POSTGRADUATE SCHOOL
March 1973

ABSTRACT

Increasing energy absorption requirements are being placed on present day aircraft carrier arresting gear engines. Hydraulic ram type engines have reached the upper limit of their development due to weight and space limitations. A turbo-type energy absorber has been proposed as an alternative. The Naval Air Engineering Center is currently developing such a machine. Theoretical analyses have determined the absorber to be practical. This study involves the testing of a flow model of that absorber with the objective to verify loss coefficients and check for flow separation in the passages. The complete model testing process is described and the desired information determined. It is recommended that further testing of off-design point performance and separation be carried out.

TABLE OF CONTENTS

LIST OF TABLES

LIST OF FIGURES

TABLE OF SYMBOLS

Symbol	Definition	Units
Latin		
A	Area	ft^2
a	Velocity of sound	ft/sec
b	Passage width, blade span	ft
C_l	Pressure loss coefficient for lower passage	- - - -
C_p	Specific heat	BTU/16/^oR
C_u	Pressure loss coefficient for upper passage	- - - -
D	Diameter of inlet pipe	ft
g	Acceleration of gravity	ft/sec^2
h	Enthalpy	ft-lb/slug
k	Blockage factor	- - - -
p	Static pressure	lb/ft^2
P_t	Total pressure	lb/ft^2
Q	Dynamic pressure	lb/ft^2
R_g	Gas constant	ft-lb/slug,^oR
r	Radius	ft
R_e	Reynolds Number	- - - -
s	Entropy	ft-lb/slug,^oR
T	Temperature	^oR
u	Internal energy	ft-lb/slug

Symbol	Definition	Units
V	Velocity	ft/sec
V_m	Meridional component of velocity	ft/sec
V_u	Peripheral component of velocity	ft/sec
$\dot{V}$	Volumetric flow rate	ft^3/sec
$\dot{w}$	Weight flow rate	lb/sec
Greek		
α	Flow angle	degree
γ	Ratio of specific heats	- - - -
δ	Non-dimensional pressure	- - - -
ζ	Total pressure less coefficient	- - - -
η_{ml}	Friction efficiency for lower passage	- - - -
η_{mu}	Friction efficiency for upper passage	- - - -
η_p	Polytropic efficiency	- - - -
θ	Non-dimensional temperature	- - - -
μ	Viscosity	$lb\text{-}sec/ft^2$
ρ	Density	lb/ft^3

Subscripts

e	Exit
i	Initial
th	Theoretical
0-10	Stations in the flow from the inlet through Station 10

ACKNOWLEDGEMENTS

The author gratefully acknowledges the assistance of Professor Michael H. Vavra. His many hours of patient direction and technical advice have proven to be of great benefit in many ways beyond simply the preparation of this thesis.

The author further wishes to acknowledge the technical help provided by Mr. James Hammer and Mr. James Selby. Their assistance was essential in the testing of the model.

I. INTRODUCTION

The general trend in the development of naval aircraft over the years has been to heavier gross weights coupled with somewhat higher approach speeds. This has forced the energy absorption capacities of carrier arresting gear to be increased. The hydraulic ram arresting gear engines in use today, however, have reached upper limit of their development from both an absorption capacity and overall size standpoint. In an effort to satisfy the ever increasing requirements placed on arresting gear engines and at the same time reduce the overall size of their installation, a totally different method of energy absorption had to be developed.

The method chosen to accomplish these goals involves the use of a rotary turbo-type energy absorber attached to a cable storage drum. The energy absorber functions by setting the working fluid in motion through the use of a rotor coupled to the cable storage drum. The fluid is subsequently retarded by a stator cascade and the resistance of the internal passages. The energy is then dissipated as heat. To achieve the constant runout characteristic required of carrier arresting gear, the fluid is merely throttled within the absorber according to the type and gross weight of the aircraft to be arrested.

The M-21 energy absorber developed in 1968 utilizes this principle but its capacity of thirty million foot-pounds is too small to warrant its use aboard ship. A program is presently underway to redesign this absorber so as to increase its capacity to fifty-five million foot-pounds. The Naval Air Engineering Center (NAEC) initiated this program with a feasibility study of the entire concept. Professor Michael H. Vavra then examined the theoretical aspects of a machine of this nature [Ref. 1].

A computer program was developed by NAEC through which the effect of various combinations of design parameters could be examined. From these data, design point parameters were chosen. Ensign Leo S. Rolek used a similar computer program to accomplish a theoretical simulation and performance analysis of the absorber [Ref. 2].

Professor Vavra was further called upon to develop and test a flow model of the absorber in an effort to refine loss estimates and check for flow separation.

In this thesis the results of the model testing will be presented. The loss coefficients determined will be compared with those assumed in the previous computer study. All data and discussion presented here apply only to design point, i.e. open throttle, performance.

II. ANALYSIS OF THE PROBLEM

The first step in any testing process is to firmly establish the goals to be accomplished. Once this is done, it can be decided what raw data must be taken to arrive at those goals and how best to obtain those data. In the present tests the main goal was the determination of experimental values for the friction efficiencies and pressure loss coefficients in the upper and lower passages of the model for comparison with the estimates used in previous computer studies. The flow would also be examined for separation at the same time.

Calculation of the coefficients is in itself an easy task. The data used in obtaining these coefficients must, however, be firmly established as being valid before any belief can be placed in the results. To verify that correct quantities were measured, it was decided to check whether conservation of mass was satisfied throughout the model, and to demonstrate that the flow was axisymmetric. Once these objectives were accomplished, a final set of detailed surveys could be taken to determine the desired coefficients.

In order to verify the axial symmetry of the flow, it was decided to compare data from three positions at each station for agreement in flow angle, velocity, and total pressure losses.

In developing the relations needed for testing, the flow was considered to be steady, two-dimensional, adiabatic and incompressible. Reynolds Number effects were not considered to be a factor. Appendix A contains a detailed development of the equations utilized for the reduction of the test data.

III. EXPERIMENTAL EQUIPMENT AND INSTRUMENTATION

The flow model tested was built by NAEC to specifications furnished by Professor Vavra. It was shipped to the Turbopropulsion Laboratory at the Naval Postgraduate School for final assembly and testing.

Suitable air flow was provided by the laboratory's main compressor. Air flow was routed from the compression aftercooler through a settling tank to a ten inch diameter inlet pipe, in an effort to insure uniform inlet conditions. The model was then attached to the inlet pipe flange.

Figure 1 is a cross section of the model showing the various stations in the flow. Six survey positions were arranged peripherally around the model, sixty degrees apart at each of stations 2, 5, 6, 9 and 10. Surveys of stations 5 and 6 are taken by inserting the probe through the same holes utilized for surveying stations 9 and 10.

There are three wall static pressure taps on each side of the passage at every station. The taps are arranged peripherally 120 degrees apart. Each group of three taps is averaged and measured against atmospheric pressure on a manometer board. These static pressures are labeled by station and whether they are situated on the inner or outer wall of the passage as shown in Figure 1.

To accomplish the flow surveys a United Sensor and Control Corporation type YC-120 three-hole probe was mounted

on a standard traverse. This allowed yaw angle as well as static and total pressure measurements to be taken. A combination total pressure and total temperature probe was placed in the inlet pipe. Both probes were connected to a water manometer board as depicted in Figure 2. This set-up allowed the necessary raw data to be collected in the simplest manner.

The techniques used in taking the flow survey were very straightforward. The probe was inserted a predetermined distance into the passage so that the probe holes lay in the plane of the inner wall. The probe was then rotated until the columns connected to each probe static tap were equal in height. This enabled flow angle to be read from the traverse rig. The manometer set-up was allowed to settle out and other data were then recorded from the manometer tubes. After all data were recorded at a point, the probe was moved to the next point and the process repeated. Survey points were taken 0.02 inches apart close to the walls and 0.1 inches apart in the center of the passage.

Lastly, all data were reduced on a Monroe model 1655 calculator utilizing the CR-1 card programmer. Probe calibration data were combined with data reduction equations and programmed into the Monroe calculator. Placing the programs on cards permitted quick and easy selection of data reduction programs.

The Monroe calculator was used exclusively throughout the project. Many functions, such as the iteration required in determining values for the polytropic efficiencies described in Appendix A, are easily and quickly accomplished due to the fact that the operator can enter the program and use his judgment and experience to effect a quick solution. This calculator, time and time again, proved itself to be an invaluable aid.

IV. THE TESTING PROCESS

Initial testing was commenced immediately upon assembly and installation of the model. The purpose of these first surveys was to insure that valid data were in fact being taken. Coarse surveys were made at three different positions for each station in the flow. The raw data were reduced to obtain flow angles and velocity profiles. The profiles at the various positions were compared in an effort to verify axisymmetry at each station in the flow. To verify continuity, the meridional velocity profiles were numerically integrated and combined with other data to arrive at flow rates which were in turn compared with flow rates determined independently by means of a standard orifice installation upstream of the model.

The results of this initial phase of testing were not good. Correlation between the two values of flow rate calculated ranged from good to poor. Comparison of profiles from several positions at the same station indicated a general lack of axisymmetry in the flow.

A quick check of all survey equipment and procedures was made in an effort to determine the cause of these poor results. It was noticed that, due to model geometry, the possibility of cross flow between stations 5, 6, 9 and 10 existed. All survey holes were then sealed. A special seal

to prevent leakage from around the tip of the probe shaft when surveying stations 5 and 6 was devised and placed into use. New surveys were then taken which produced only slightly better results. No real progress was made, however.

From this point in the testing process, all possible efforts were concentrated on merely obtaining reasonable results from the model. The next step was to shift from dimensional mass flow rates to the referred mass flow rates developed in Appendix A. This eliminated temperature and barometric effects from the results. The use of referred flow rates tended to smooth out the results somewhat; however, they were not yet satisfactory.

Next, a two-fold program was begun. For ease in the determination and observation of flow rates, it was decided to develop a plot of referred mass flow rate, as measured by the orifice, versus a pressure ratio of inlet total pressure to atmospheric pressure. At the same time, the initial assumption that Reynolds Number effects on model efficiency were negligible was challenged. Appendix A contains the development of the polytropic efficiency and Reynolds Number terms used in this test. A run was then made by varying flow rate from its lowest practical value to the upper limits of the compressor. The results of this run are depicted in Figure 3 and Figure 4. Figure 4 verified the assumption that Reynolds Number effects on efficiency are indeed negligible.

Figure 3, however, disclosed non-linearity in referred mean flow rate below an inlet pressure ratio of 1.09. As all previous survey data were taken with inlet pressure ratios in this range, it was decided to use higher flow rates for all future surveys. In an effort to more closely monitor flow rate for possible variations, the survey equipment was altered to include the inlet total pressure probe as shown in Figure 2. All subsequent survey data included inlet pressure ratio which was used in conjunction with Figure 3 to obtain flow rate measurements.

A series of runs was then initiated utilizing all improvements and refinements made to date. Inlet pressure ratios were maintained above 1.09. The new survey set-up was used in conjunction with the internal seals. Referred mass flow rates were used exclusively and were closely monitored for variation throughout the entire process. Another check for continuity and axisymmetry was made by using the new data. The results once more indicated small improvement; however, unacceptable discrepancies still existed.

It was then decided that the model itself would have to be carefully examined to the point of disassembly, in an effort to determine the reasons for the poor results. All internal passages were again measured for uniformity and leakage. All appeared to be in order. Upon disassembly of the model however, several discrepancies came to light.

The inlet flange of the model was not precisely aligned with the inlet pipe. Further, the inlet bell mouth in the settling tank exit had fallen off at some prior time. These two factors combined to produce a non-uniform inlet condition. Further, two pieces of friction tape, each approximately one inch long, were found within the model itself, no doubt contributing to the apparent non-axisymmetric flow. Lastly and most important, from dust traces on the internal passage walls, it could readily be seen that the survey hole positions were not located properly with respect to the blade rows. In fact, some survey holes were situated directly in blade wakes. The stator cascade was by far the worst, having to be rotated through a distance of roughly one half of a blade spacing to obtain a satisfactory relationship between the cascade and the survey positions.

These discrepancies were corrected and the model carefully rebuilt. Another series of runs was then undertaken on the rebuilt model utilizing all the improvements made up to that time. The results of the test for axisymmetry depicted in Figure 5 through Figure 19, were excellent. Flow rate comparisons were also in good agreement, with the exception of station 5 which indicated a flow rate some six percent less than the orifice flow rate.

The discrepancy in flow rate at station 5 was determined to be caused by difficulties in properly measuring flow angle

at the stator inlet. When the stator cascade had been rotated to its optimum position with respect to the survey holes, in particular the holes at station 6, it was noted that the survey holes at station 5 were very close to the leading edges of the stator blades. The upstream influence of the flow around the stator blades, no doubt caused by the large pressure drop across the stator cascade shown in Figure 20, caused larger than average flow angles to be measured because of the situation illustrated in Figure 21.

Calculations were made again for station 5, utilizing flow angles arbitrarily selected to be two degrees less than those actually measured. The results of these calculations disclosed a difference of less than two percent between the two flow rates. Valid results were now believed to be obtainable from the model.

After this verification, detailed surveys were finally taken at one position for each station. Station 10 was omitted altogether as it has no bearing on actual results. The results of this final run are shown in Table I and Figure 22 through Figure 37.

TABLE I

SUMMARY OF FLOW RATE COMPARISONS

	Calculated Referred Flow Rate	Orifice Referred Flow Rate	Percentage Difference
Station 2	5.43	5.39	+0.7%
Station 5	5.37	5.45	-1.5%
Station 6	5.42	5.38	+0.7%
Station 9	5.24	5.42	-3.3%

V. RESULTS AND DISCUSSION

Analysis of the final run data yielded the results listed in Table II. The data assumed by Rolek [Ref. 2] are also listed for comparison.

TABLE II

SUMMARY OF RESULTS

	η_{mu}	η_{ml}	C_u	C_l
Experimental	0.942	0.827	0.487	1.75
Assumed [Ref. 2]	0.782	0.876	0.436	0.515

It can be noted that the difference between the assumed and the experimentally obtained coefficients is small, with the exception of the lower passage pressure loss coefficient.

Examination of Figures 25, 29, 33 and 37 reveals the strong possibility that separation has occurred prior to station 9, which is confirmed by Figure 20. At station 7-outer, the wall static pressure is greater than that at station 7-inner. This is exactly the opposite from what one would expect of normal attached flow. Furthermore, the pressures at station 8 are very nearly equal, suggesting that separation has already occurred prior to station 8-outer. Obviously, if separation occurs, the pressure loss coefficient will be increased considerably. At present, thorough investigation of

this lower passage is not possible; however, it is felt that the high experimental value of C_1 is caused by separation in the lower passage.

An important factor in considering the results obtained for the lower passage is the uniformity of the flow at station 6. In the model, the lower passage is of necessity curved in the opposite direction from that in the actual machine. If the flow in the model at station 6 were non-uniform, the turning effects of the model's reversed lower passage would render any data taken downstream of it invalid. Since this is not the base, credence can be given to the experimental results.

It is noteworthy here that no one single factor seemed to prevent good data from being obtained. Certainly some discrepancies had a larger effect on the results than others; however, they all acted together to complicate testing. Meticulous attention to detail was necessary to obtain good results. Only through the use of a systematic approach to troubleshooting, utilizing sound logic and proven experimental methods, were the obstacles determined and overcome. That success was obtained only through the application of sound engineering principles in problem solution cannot be emphasized enough.

VI. CONCLUSIONS AND RECOMMENDATIONS

The primary conclusion of this thesis is that the final results are sound; hence, the experimental coefficients listed in Table II are valid.

It is recommended that testing of the model's off-design performance be initiated utilizing the procedures established herein. Following careful installation of the throttle ring, coarse surveys should be taken at several positions for each station in order to establish the axisymmetry of the flow. After this condition has been verified, detailed surveys can be taken at each station to establish the required coefficients.

It is recommended further that a survey station be established at or near station 8 for further investigation of separation in the lower passage. If axisymmetry is first established, this would entail the addition of only one position. Investigation of conditions at station 8 would be most beneficial to study the flow conditions in the lower passage.

APPENDIX A

DEVELOPMENT OF EQUATIONS USED IN DATA REDUCTION

1. Reynolds Number Effects

Figure 38 is a temperature-entropy diagram for an adiabatic process with friction. From the first law of thermodynamics

$$T\,ds = du + p\,dv \tag{1}$$

This may be written as

$$T\,ds = dh - v\,dp \tag{2}$$

With the perfect gas equation and the definition of enthalpy

$$ds = C_p \frac{dT}{T} - R_g \frac{dp}{p} \tag{3}$$

and

$$C_p = \frac{\gamma}{\gamma-1} R_g \tag{4}$$

Substituting Equation (4) into Equation (3) and rearranging, gives

$$\frac{ds}{R_g} = \frac{\gamma}{\gamma-1} \frac{dT}{T} - \frac{dp}{p} \tag{5}$$

From this equation and Figure 38, it can be seen that for and isentropic process from T to T_{is}

$$d\,T_{is} = \frac{\gamma-1}{\gamma}\,T\,\frac{dp}{p} \tag{6}$$

The polytropic efficiency is now defined as

$$\eta_p = \frac{dT}{dT_{is}} \tag{7}$$

Substituting this definition into Equation (6) yields

$$\frac{dT}{T} = \eta_p\,\frac{\gamma-1}{\gamma}\,\frac{dp}{p} \tag{8}$$

Equation (8) can now be integrated to give

$$\ln T = \ln p^{\eta_p(\frac{\gamma-1}{\gamma})} \tag{9}$$

If the process is referenced to some reference state '0', Equation (9) becomes

$$\frac{T}{T_{to}} = \left(\frac{p}{p_{to}}\right)^{\eta_p(\frac{\gamma-1}{\gamma})} \tag{10}$$

Now, for an adiabatic process

$$\frac{V^2}{2gC_p} = T_{to} - T \tag{11}$$

Substitution of Equation (4) into Equation (11) and re-arrangement yields

$$V^2 = 2g \frac{\gamma}{\gamma-1} R_g T_{to} \left(1 - \frac{T}{T_{to}}\right) \tag{12}$$

With the weight flow rate $\dot{w}$

$$\dot{w} = \frac{A V}{v} \tag{13}$$

From perfect gas relations, specific volume can be expressed by

$$v = \frac{R_g T}{p} \tag{14}$$

Equations (12) and (14) substituted into Equation (13) yield

$$\dot{w}^2 = \frac{A^2 V^2}{v^2} = A^2 2g \frac{\gamma}{\gamma-1} R_g T_{to} \left(1 - \frac{T}{T_{to}}\right) \frac{p^2}{R_g^2 T^2} \frac{v_o^2}{v_o^2} \tag{15}$$

Rearranging

$$\frac{\dot{w}^2 v_o^2}{A^2} = 2g \frac{\gamma}{\gamma-1} R_g T_{to} \left(1 - \frac{T}{T_{to}}\right) \frac{p^2}{R_g^2 T^2} \left(\frac{R_g^2 T_{to}^2}{P_{to}^2}\right) \tag{16}$$

or

$$\frac{\dot{w}^2 R_g^2 T_{to}^2}{P_{to}^2 A^2 g R_g T_{to}} = \frac{2\gamma}{\gamma-1} \frac{\left(\frac{p}{P_{to}}\right)^2}{\left(\frac{T}{T_{to}}\right)^2} \left(1 - \frac{T}{T_{to}}\right) \tag{17}$$

Further substitution of Equation (10) into Equation (17) gives

$$\frac{\dot{w}^2 R_g/g T_{to}}{P_{to}^2 A^2} = \frac{2\gamma}{\gamma-1}\frac{(p/P_{to})^2}{(p/P_{to})^{2\eta_p(\frac{\gamma-1}{\gamma})}}\left[1-(\frac{p}{P_{to}})^{\eta_p\frac{\gamma-1}{\gamma}}\right] \quad (18)$$

Equation (18) now contains only known or easily measured quantities; however, for ease of calculation, the left hand side will now be reduced to a referred weight flow rate using the NASA definitions θ and δ .

The non-dimensional temperature and pressure terms are defined as

$$\theta = \frac{T_{to}}{518.4} \quad (19)$$

$$\delta = \frac{P_{to}}{14.7} \quad (20)$$

The substitution of these definitions into and further simplification of Equation (18) yields

$$\frac{\dot{w}\sqrt{\theta}}{\delta} = 14.7A\left\{\frac{g}{518.4R_g}\frac{2\gamma}{\gamma-1}\left[(\frac{p}{P_{to}})^{2-2\eta_p(\frac{\gamma-1}{\gamma})} - (\frac{p}{P_{to}})^{2-\eta_p(\frac{\gamma-1}{\gamma})}\right]\right\}^{1/2} \quad (21)$$

Equation (21) was programmed into the Monroe 1655 and the values of η_p calculated by trial and error for the various data points taken. To determine the Reynolds Number

corresponding to these polytropic efficiencies, the following was defined

$$R_e = \frac{VD\rho}{\mu} \tag{22}$$

where the terms refer to velocity, diameter, density, and viscosity at the inlet to the model. Further, the mass flow rate at the inlet may be written

$$\dot{w} = k \frac{\pi}{4} D^2 V \frac{P_o}{R_g T_o} \tag{23}$$

where k is a blockage factor. Solving Equation (23) for velocity, and substituting this result into Equation (22) gives

$$R_e = \frac{\dot{w} \quad 4}{Dk\pi\mu \quad g} \tag{24}$$

Rearranging Equation (24)

$$R_e g \frac{\pi}{4} D\mu h = \left(\frac{\dot{w}\sqrt{\theta}}{\delta}\right) \frac{\delta}{\sqrt{\theta}} \tag{25}$$

Noting that the left hand side of Equation (25) is still non-dimensional, a new Reynolds Number, say R_e^* can be defined such that

$$R_e^* = R_e g \frac{\pi}{4} Dk\mu \tag{26}$$

and then by Equation (25)

$$R_e^* = \frac{\dot{w}\sqrt{\theta}}{\delta} \left(\frac{\delta}{\sqrt{\theta}}\right) \tag{27}$$

Equation(27) is in terms of the referred flow rate so that R_e^* may be determined easily.

2. Velocity measurement

The stagnation process at a probe tip can be described by the same equations used previously in the treatment of an adiabatic process with friction. Now, assuming the stagnation process to be frictionless, Equations (10) and (12) combine to yield

$$V^2 = 2gR_g \frac{\gamma}{\gamma-1} T_t \left[1 - \left(\frac{p}{P_t}\right)^{\frac{\gamma-1}{\gamma}}\right] \tag{28}$$

Now let

$$p = P_t - Q \tag{29}$$

This allows Equation (28) to be written

$$V^2 = 2gR_g \frac{\gamma}{\gamma-1} T_t \left[1 - \left(1 - \frac{Q}{P_t}\right)^{\frac{\gamma-1}{\gamma}}\right] \tag{30}$$

Equation (3) provides an efficient and quick means for obtaining velocities. It also requires a minimum amount of data collection. All velocity data utilized in the final run were computed with this equation. An even more

appropriate method was used in obtaining velocity profiles for comparison in the test for axisymmetry. The velocity of sound at T_t can be written

$$a_t = \sqrt{\gamma R_g g T_t} \tag{31}$$

Substitution of this into Equation (30) yields a dimensionless velocity ratio

$$\left(\frac{V}{a_t}\right)^2 = \frac{2}{\gamma-1}\left[1 - \left(1 - \frac{Q}{P_t}\right)^{\frac{\gamma-1}{\gamma}}\right] \tag{32}$$

This equation requires even fewer raw data than Equation (30). It could be easily approximated by the use of a series expansion; however, the versatility and accuracy of the Monroe calculator makes this unnecessary.

If the total velocity is obtained, the peripheral and meridional components, V_u and V_m, are found with the measured flow angle, or

$$V_m = V \cos \alpha \tag{33}$$

$$V_u = V \sin \alpha \tag{34}$$

3. Referred Flow Rates

To check continuity, the meridional velocities are integrated across the known passage width.

Volumetric flow rate can be written

$$\forall = 2\pi r \int_0^b V_m \, dx \tag{35}$$

where r is the radius at that station and b is the passage width. From this volumetric flow rate, the weight flow rate $\dot{w}$ is obtained by

$$\dot{w} = \frac{P}{R_g T} 2\pi r \int_0^b V_m \, dx \tag{36}$$

Equation (36) is finally transformed into a referred mass flow rate through the substitution of Equations (19) and (20), or

$$\frac{\dot{w}\sqrt{\theta}}{\delta} = \sqrt{\frac{T_{to}}{518.4}} \; \frac{P_{to}}{14.7} \; \frac{p}{R_g T} 2\pi r \int_0^b V_m \, dx \tag{37}$$

In reducing the data presented in this thesis, a weighted average of the static pressures recorded at each point in the survey was used. Simpson's Rule was utilized to obtain the meridional velocity integral.

4. Total Pressure Loss Coefficient

Total pressure losses were examined to help verify the axisymmetry of the flow as well as the general validity of the raw data obtained. These losses were represented in the

form of a non-dimensional coefficient referenced to the inlet total pressure. The total pressure loss coefficient at some position 'i' is defined as

$$\zeta_{o-i} = \frac{P_{to} - P_{ti}}{P_{to}} \tag{38}$$

5. Pressure Loss Coefficient

The definition of the pressure loss coefficient was established by Vavra [Ref. 1] as

$$\frac{(\bar{p}_e)_{th}}{\rho} - \frac{\bar{p}_e}{\rho} = C_{u/l} \frac{\bar{V}_{me}^2}{2} \tag{39}$$

This must now be rearranged to include only known or easily measured quantities. The definition of total pressure is

$$\frac{(\bar{P}_{te})_{th}}{\rho} = \frac{(\bar{p}_e)_{th}}{\rho} + \frac{1}{2} (\bar{V}_{me})^2 + \frac{1}{2} (\bar{V}_{ue})^2 \tag{40}$$

Assuming no losses, there must be for any passage

$$(\bar{P}_{te})_{th} = \bar{P}_{ti} \tag{41}$$

Substituting Equation (41) into Equation (40) yields

$$\frac{\bar{P}_{e_{th}}}{\rho} = \frac{\bar{P}_{ti}}{\rho} - \frac{1}{2} (\bar{V}_{me})^2 - \frac{1}{2} (\bar{V}_{ue})^2 \tag{42}$$

By Equation (40), the average static pressure at the passage exit is

$$\frac{\bar{P}_e}{\rho} = \frac{\bar{P}_{te}}{\rho} - \frac{1}{2}(\bar{V}_{me})^2 - \frac{1}{2}(\bar{V}_{ue})^2 \qquad (43)$$

Substituting Equation (42) and Equation (43) into Equation (39) and solving for $C_{u/1}$ yields

$$C_{u/1} = \frac{\bar{P}_{ti} - \bar{P}_{te}}{\frac{\rho}{2}(\bar{V}_{me})^2} \qquad (44)$$

6. Friction Efficiency

The friction efficiency, η_m, was defined by Vavra [Ref. 1] as

$$\bar{V}_{ue} = \eta_m \bar{V}_{ue_{th}} = \eta_m \bar{V}_{ui} \qquad (45)$$

7. Mass Averaged Quantities

The velocity and total pressure values required in Equation (44) and Equation (45) are mass averaged values. The method of calculating one of these values is developed here, the other quantities are obtained in a similar manner.

For mass averaged peripheral velocities at station 'i'

$$\bar{V}_{ui} = \frac{\int d\dot{m}_i \, V_{ui}}{\int d\dot{m}_i} \qquad (46)$$

The differential mass flow rate can be written

$$d\dot{m}_i = \rho\, 2\pi\, R_i\, V_{mi}\, dx \tag{47}$$

Therefore, removing constants,

$$d\dot{m}_i\, V_{ui} = \rho\, 2\pi\, R_i \int V_{ui} V_{mi}\, dx \tag{48}$$

Equation (47) and Equation (48) are now substituted into Equation (46) to yield

$$\bar{V}_{ui} = \frac{\int V_{ui}\, V_{mi}\, dx}{\int V_{mi}\, dx} \tag{49}$$

similarly,

$$\bar{V}_{ue} = \frac{\int V_{ue}\, V_{me}\, dx}{\int V_{me}\, dx} \tag{50}$$

$$\bar{V}_{me} = \frac{\int V_{me}^{\,2}\, dx}{\int V_{me}\, dx} \tag{51}$$

$$\bar{P}_{ti} = \frac{\int P_{ti}\, V_{mi}\, dx}{\int V_{mi}\, dx} \tag{52}$$

$$\bar{P}_{te} = \frac{\int P_{te}\, V_{me}\, dx}{\int V_{me}\, dx} \tag{53}$$

The above integrations were carried out numerically on the Monroe 1655 calculator by using Simpson's Rule.

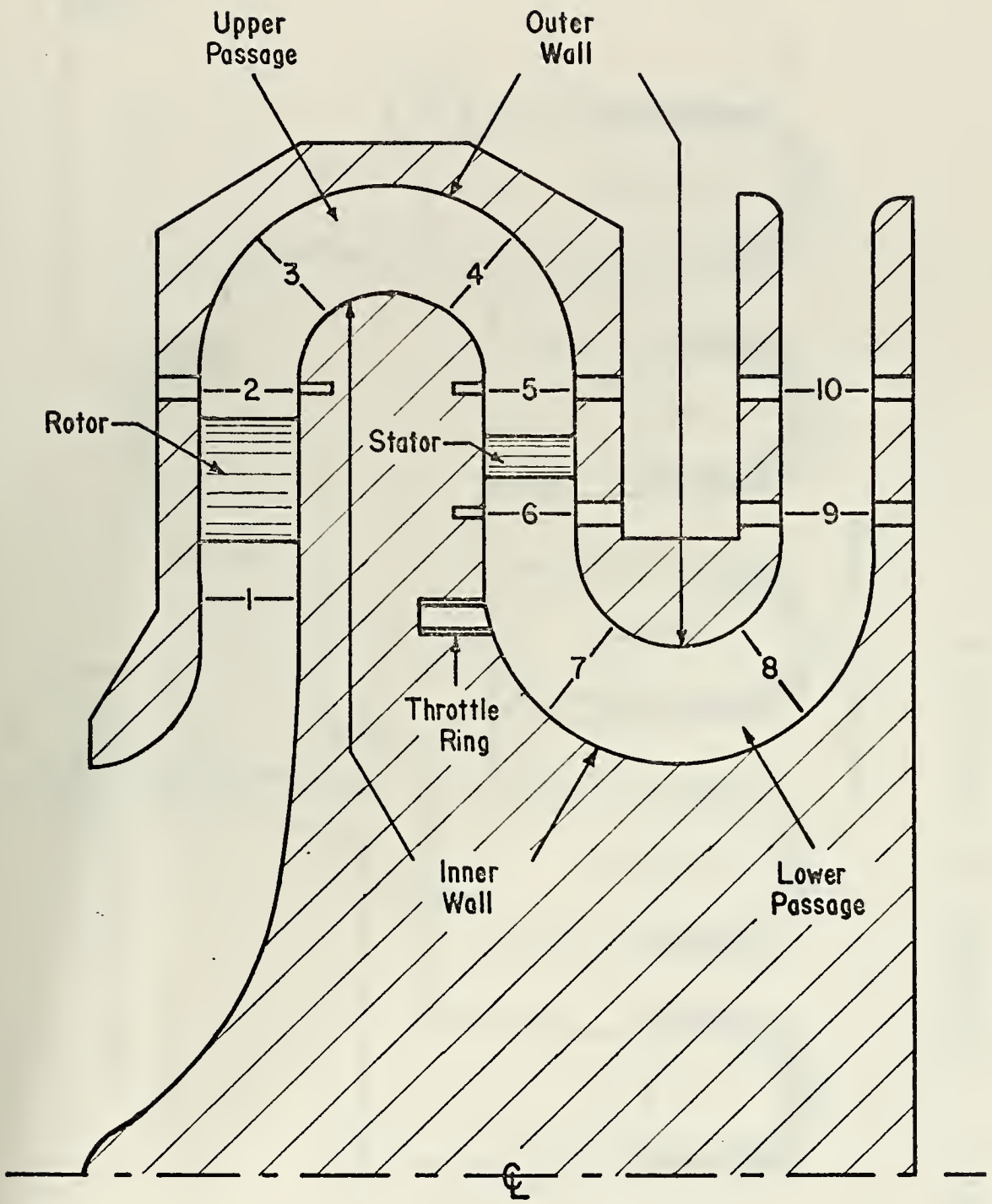

Figure 1 Cross Section of Flow Model

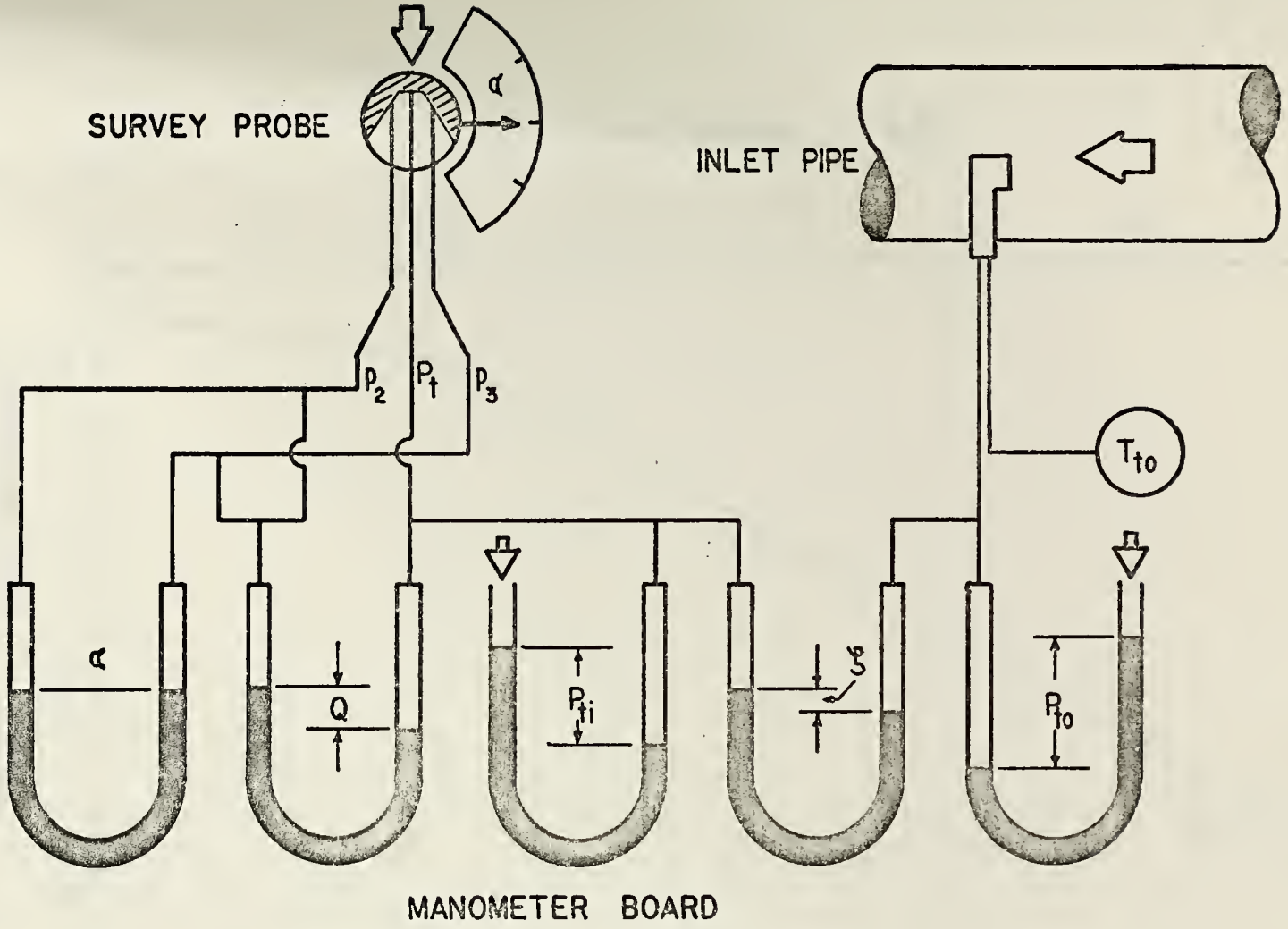

Figure 2 Schematic of Survey Rig

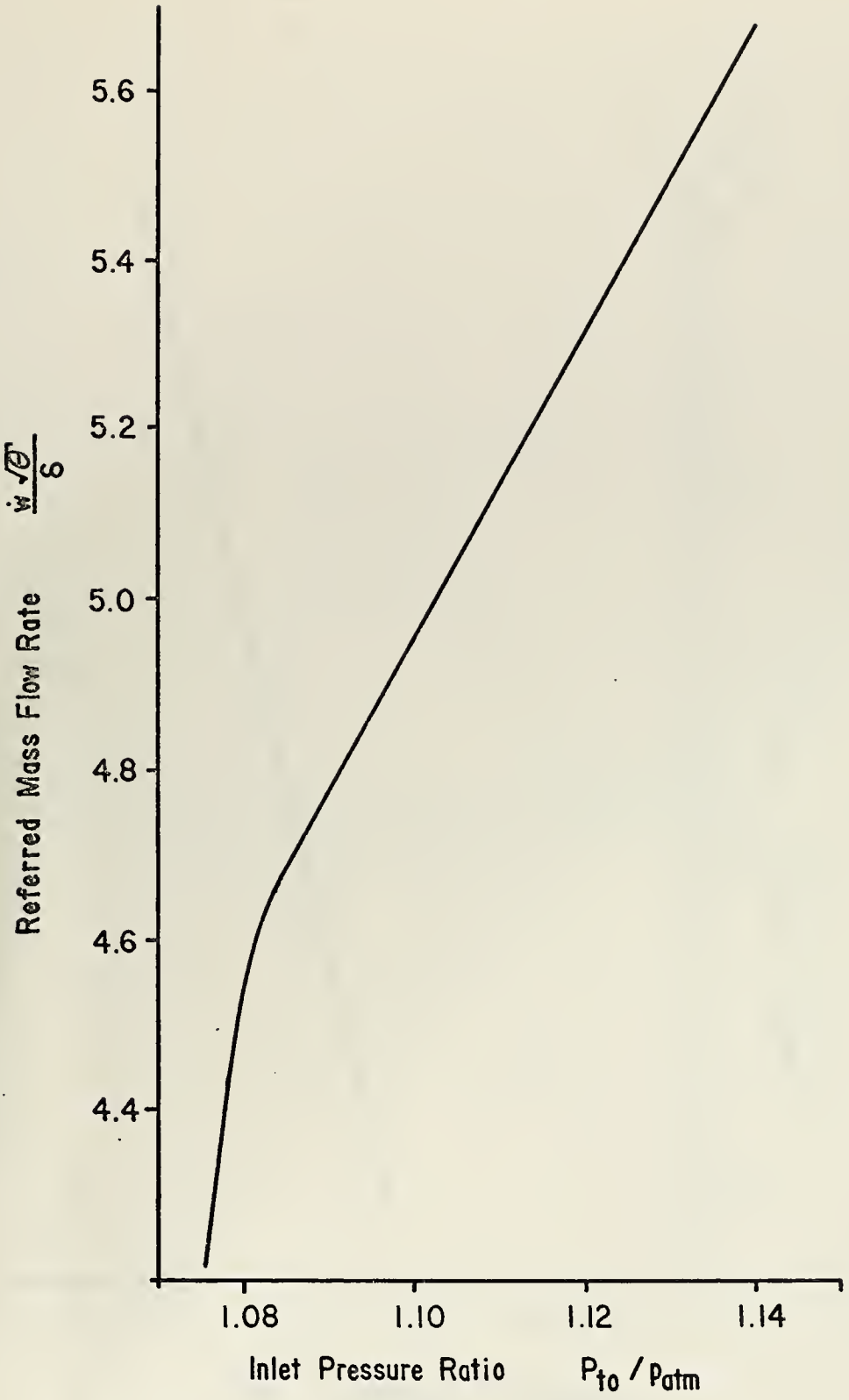

Figure 3 Referred Mass Flow Rate versus Inlet Pressure Ratio

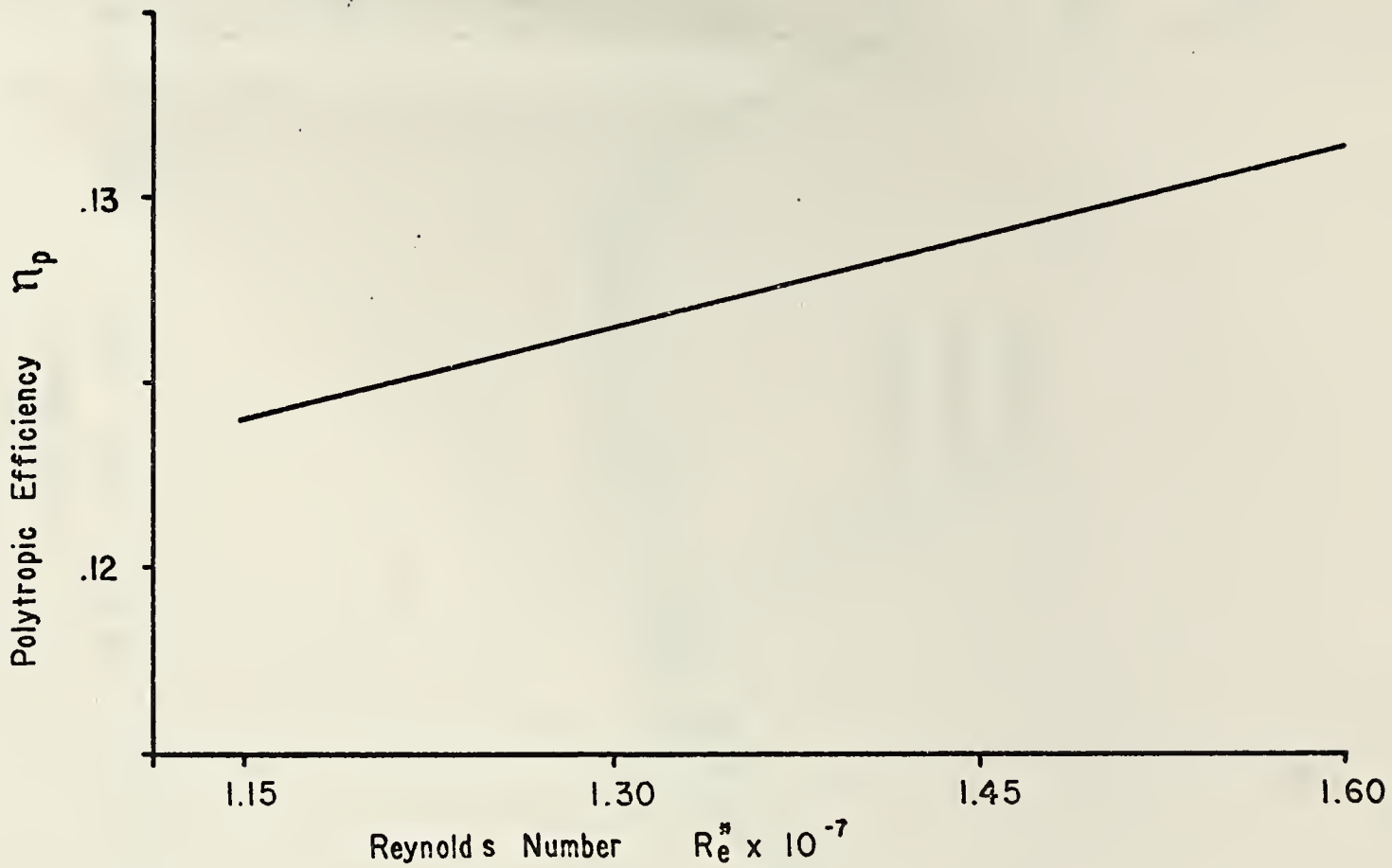

Figure 4 Polytropic Efficiency versus Reynold's Number

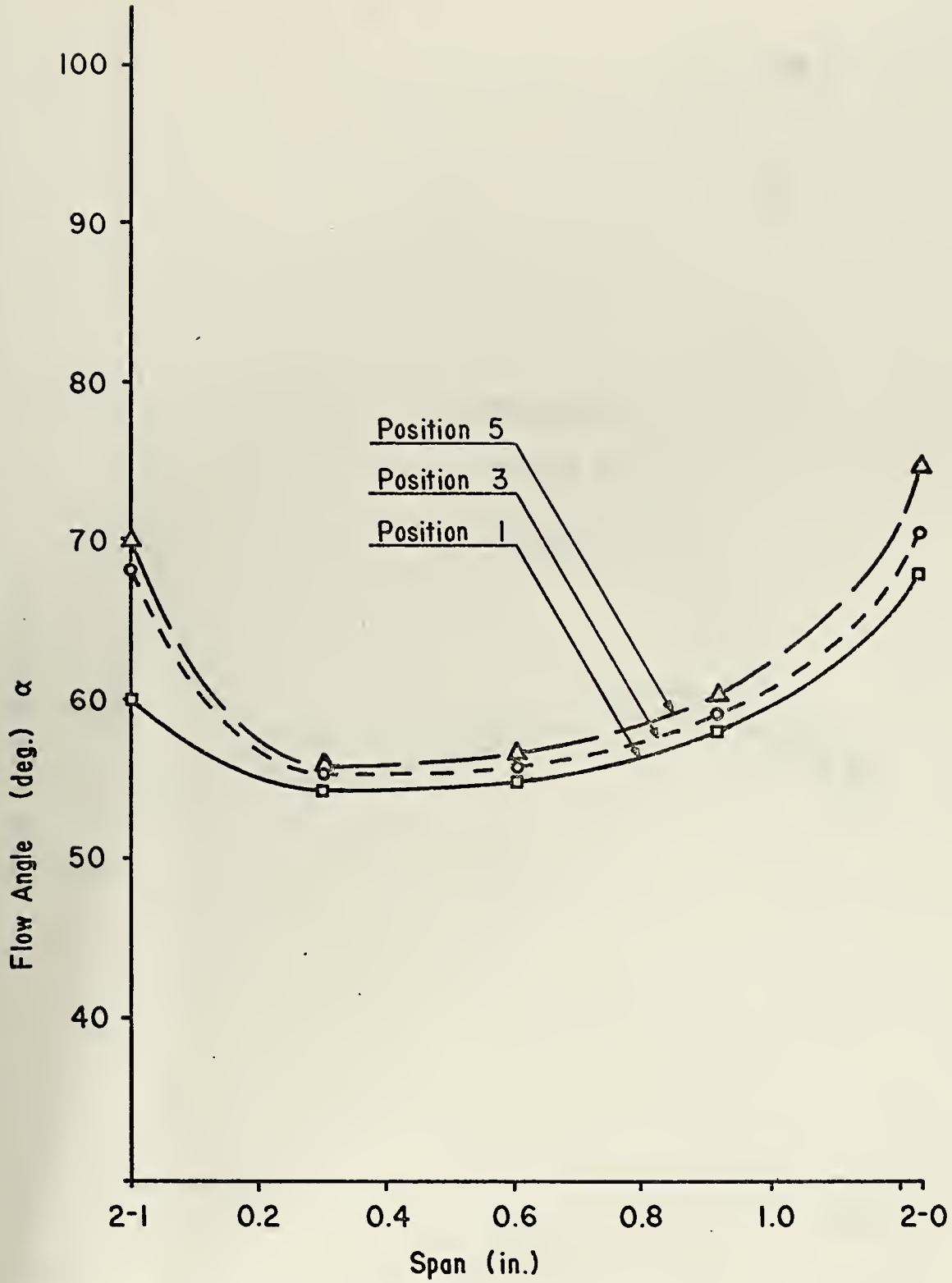

Figure 5 Flow Angle versus Span at Station 2 (coarse)

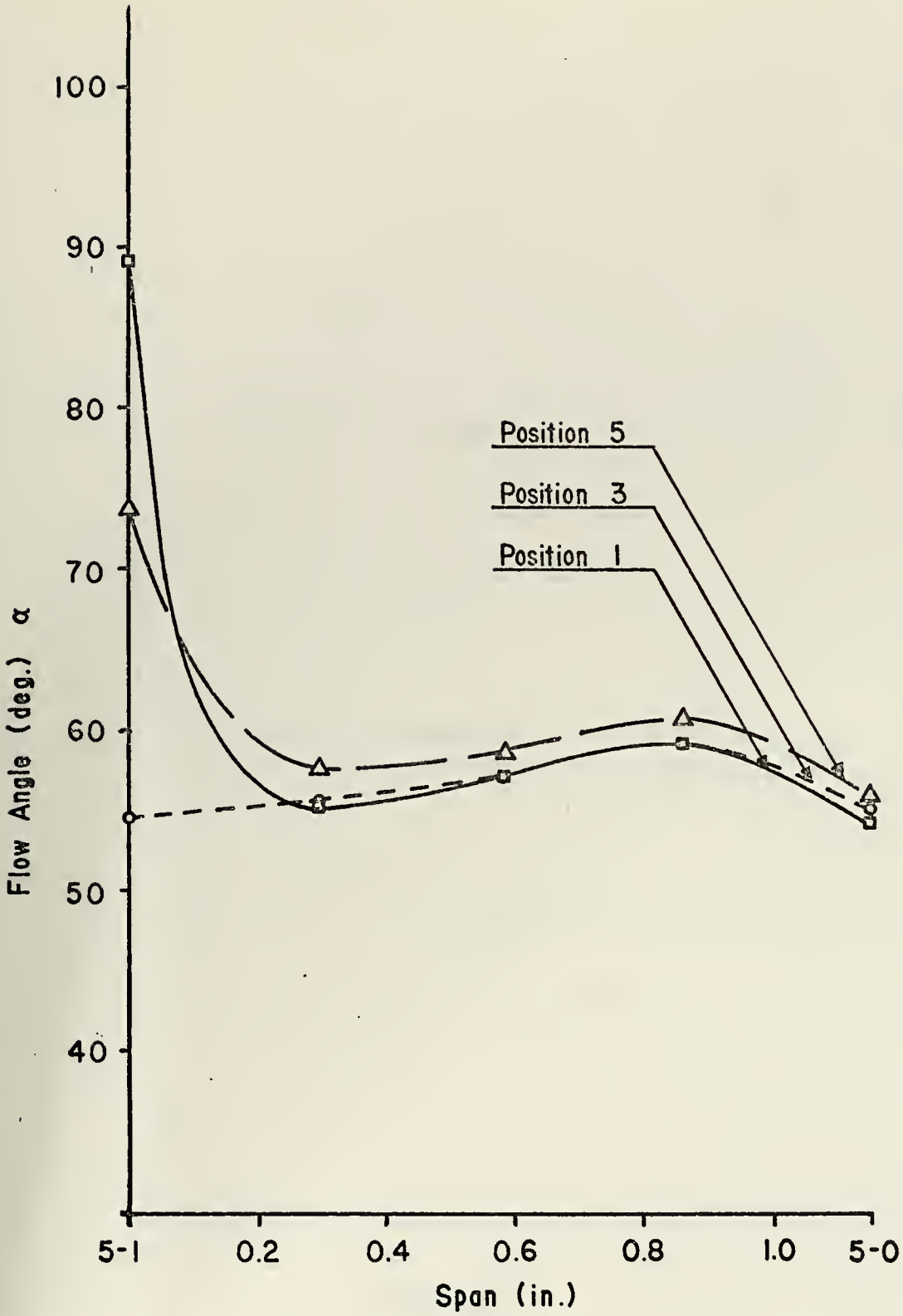

Figure 6 Flow Angle versus Span at Station 5 (coarse)

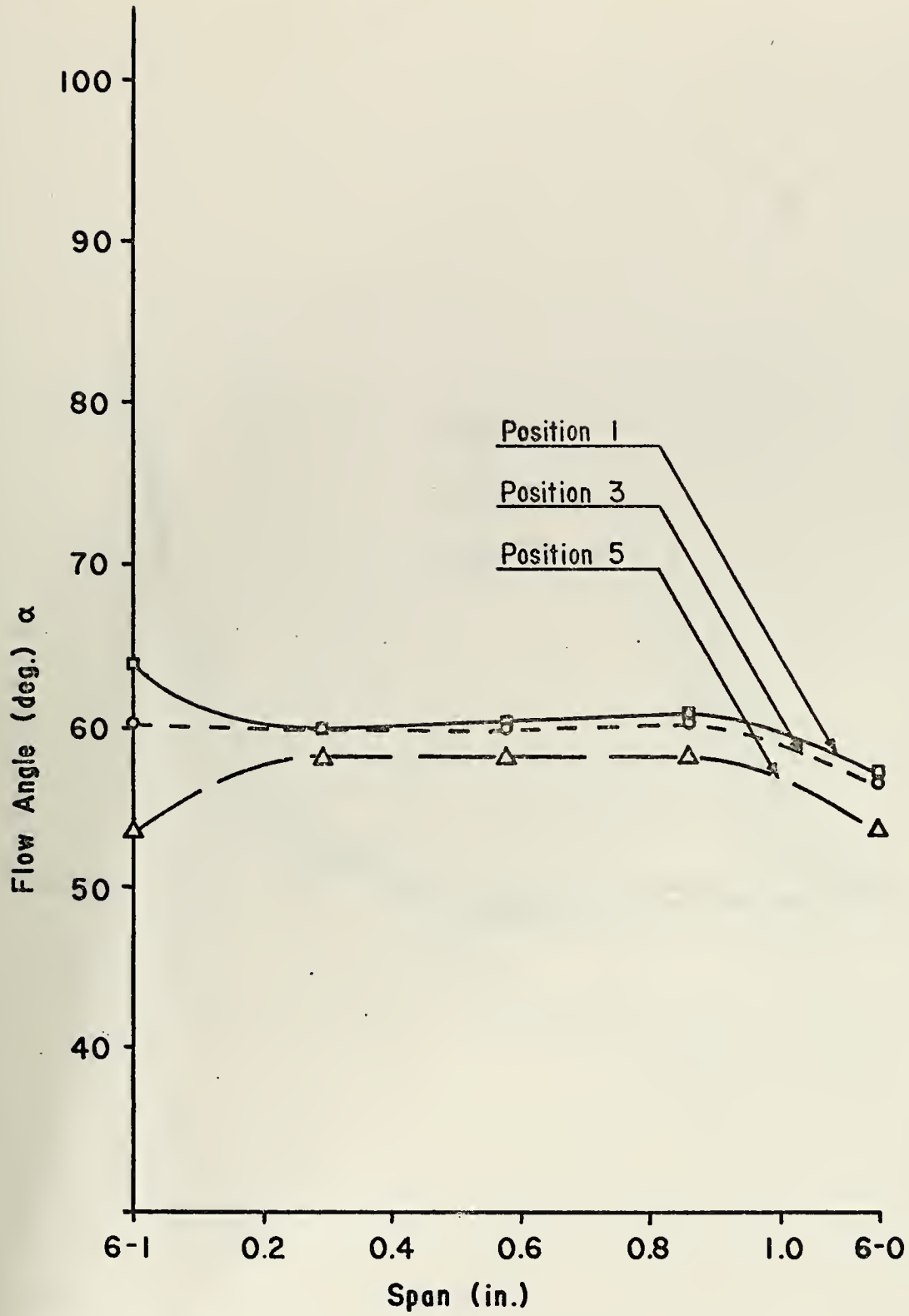

Figure 7 Flow Angle versus Span at Station 6 (coarse)

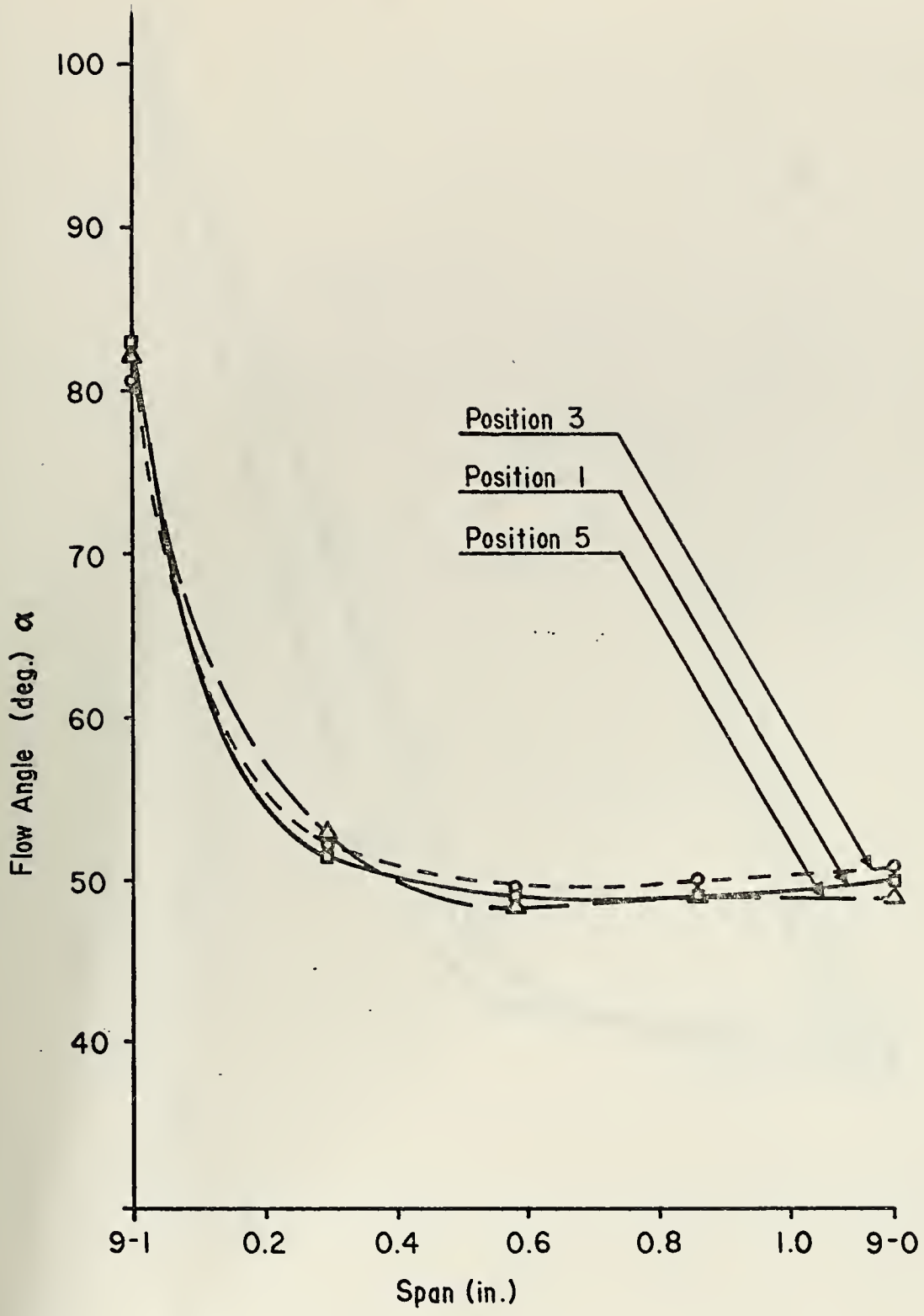

Figure 8 Flow Angle versus Span at Station 9 (coarse)

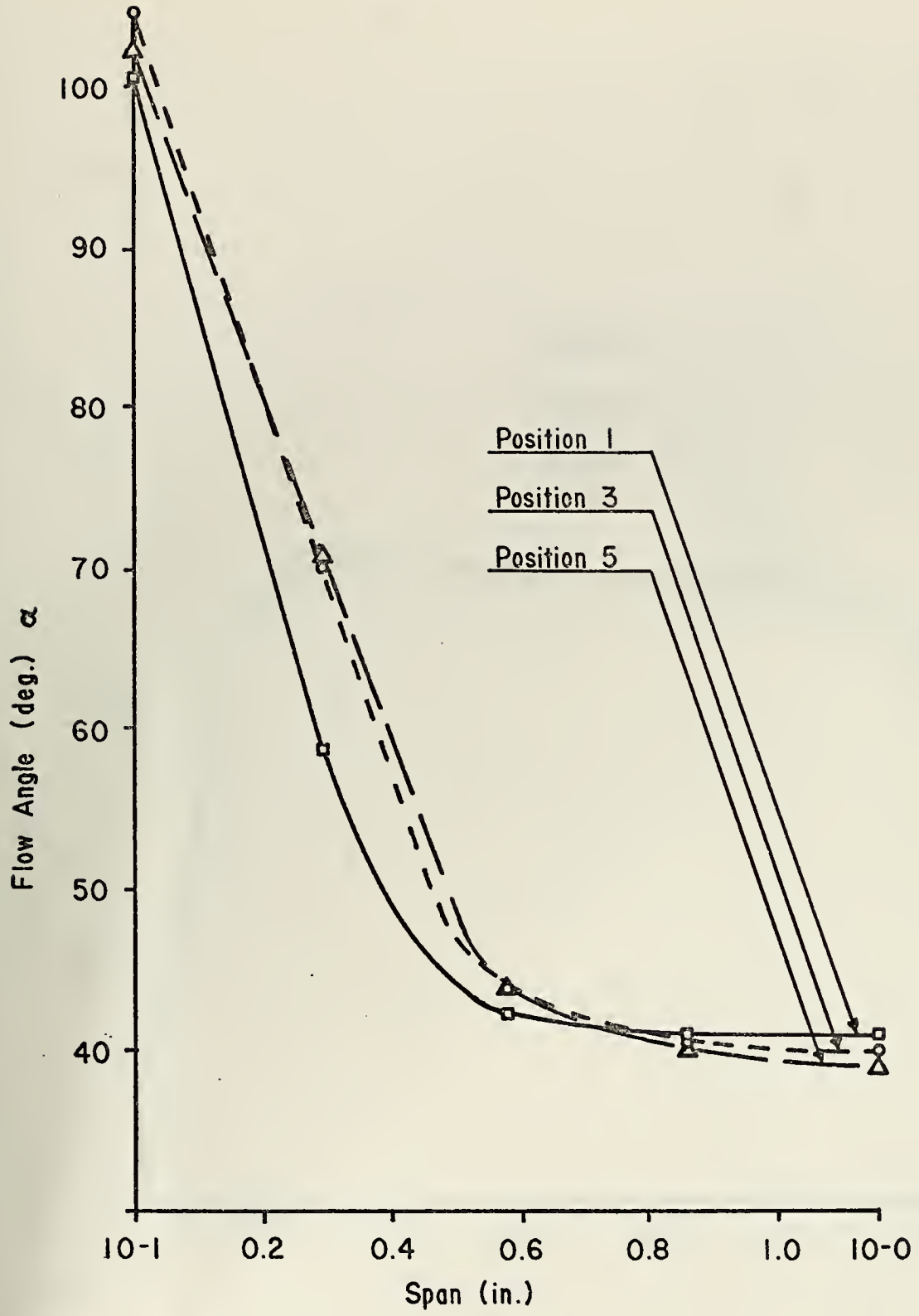

Figure 9 Flow Angle versus Span at Station 10 (coarse)

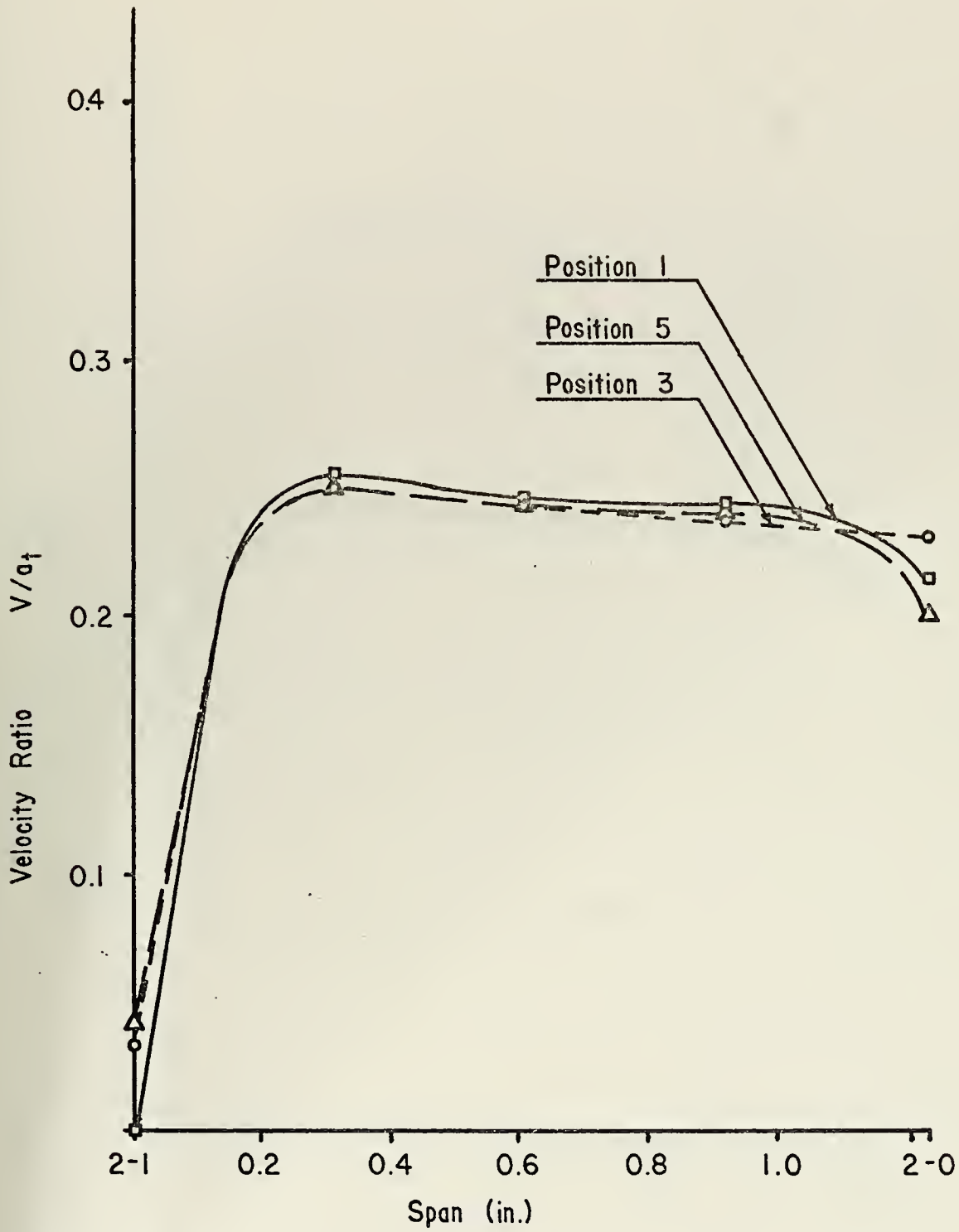

Figure 10 Velocity Ratio versus Span at Station 2 (coarse)

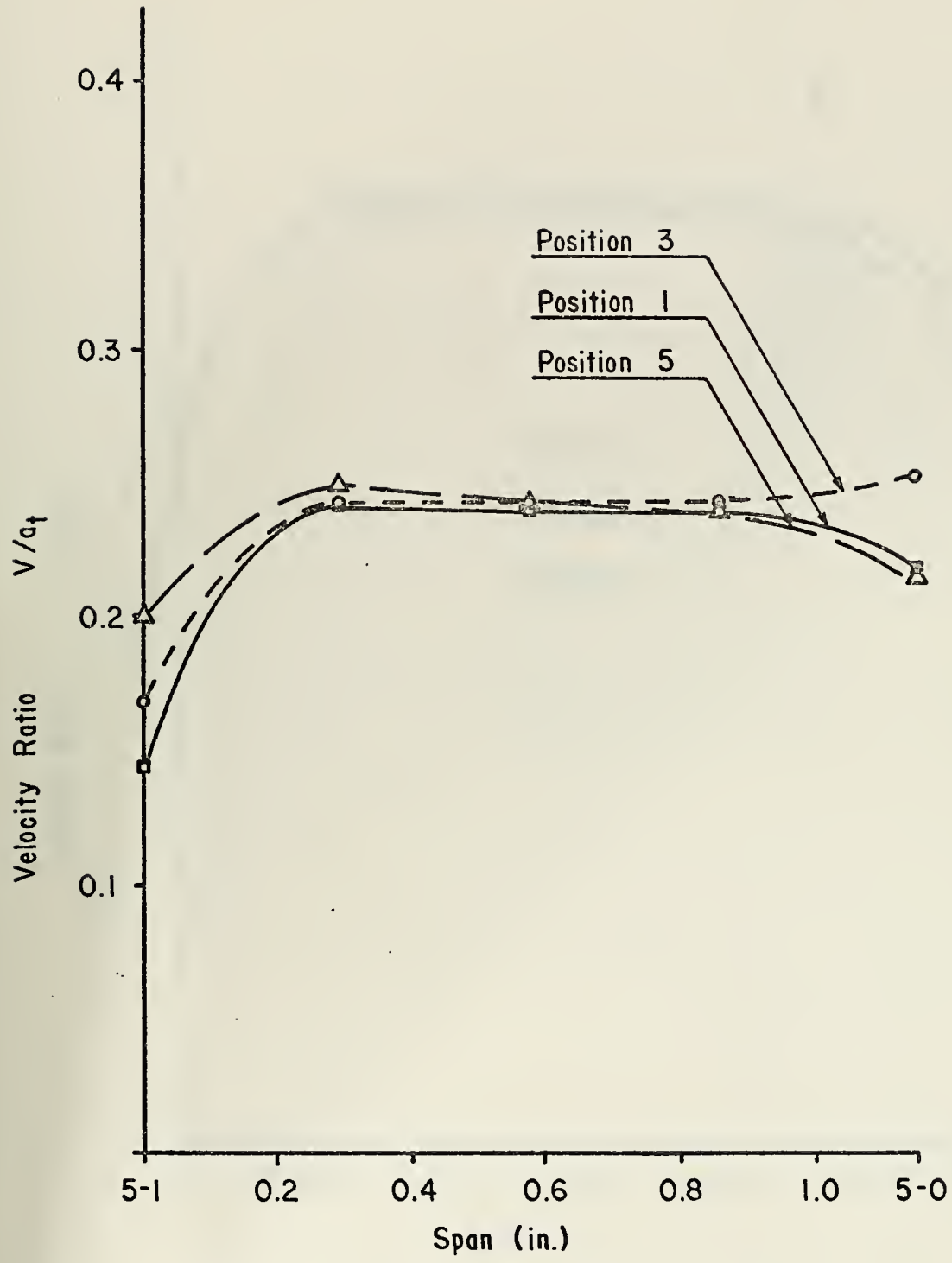

Figure 11 Velocity Ratio versus Span at Station 5 (coarse)

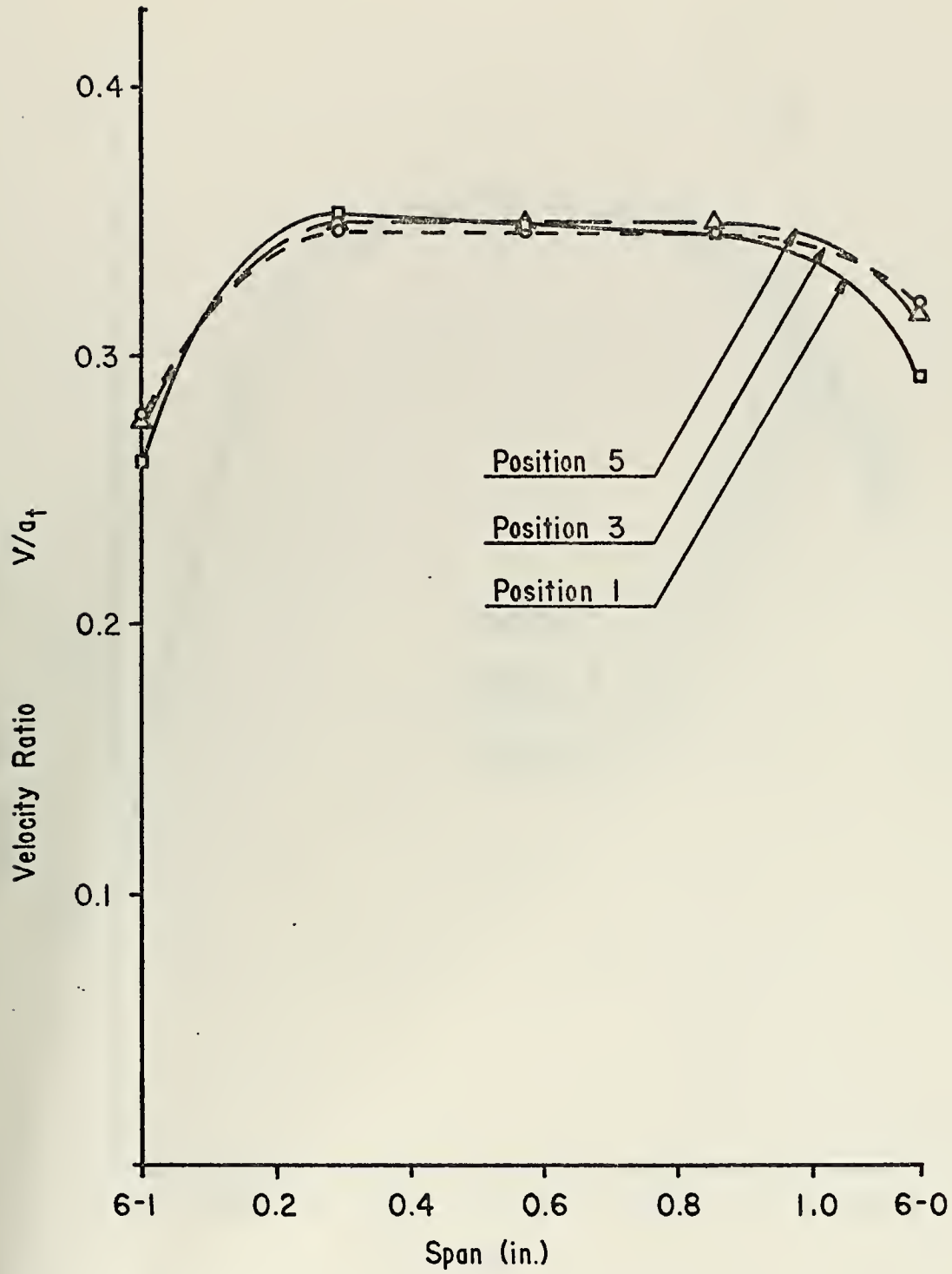

Figure 12 Velocity Ratio versus Span at Station 6 (coarse)

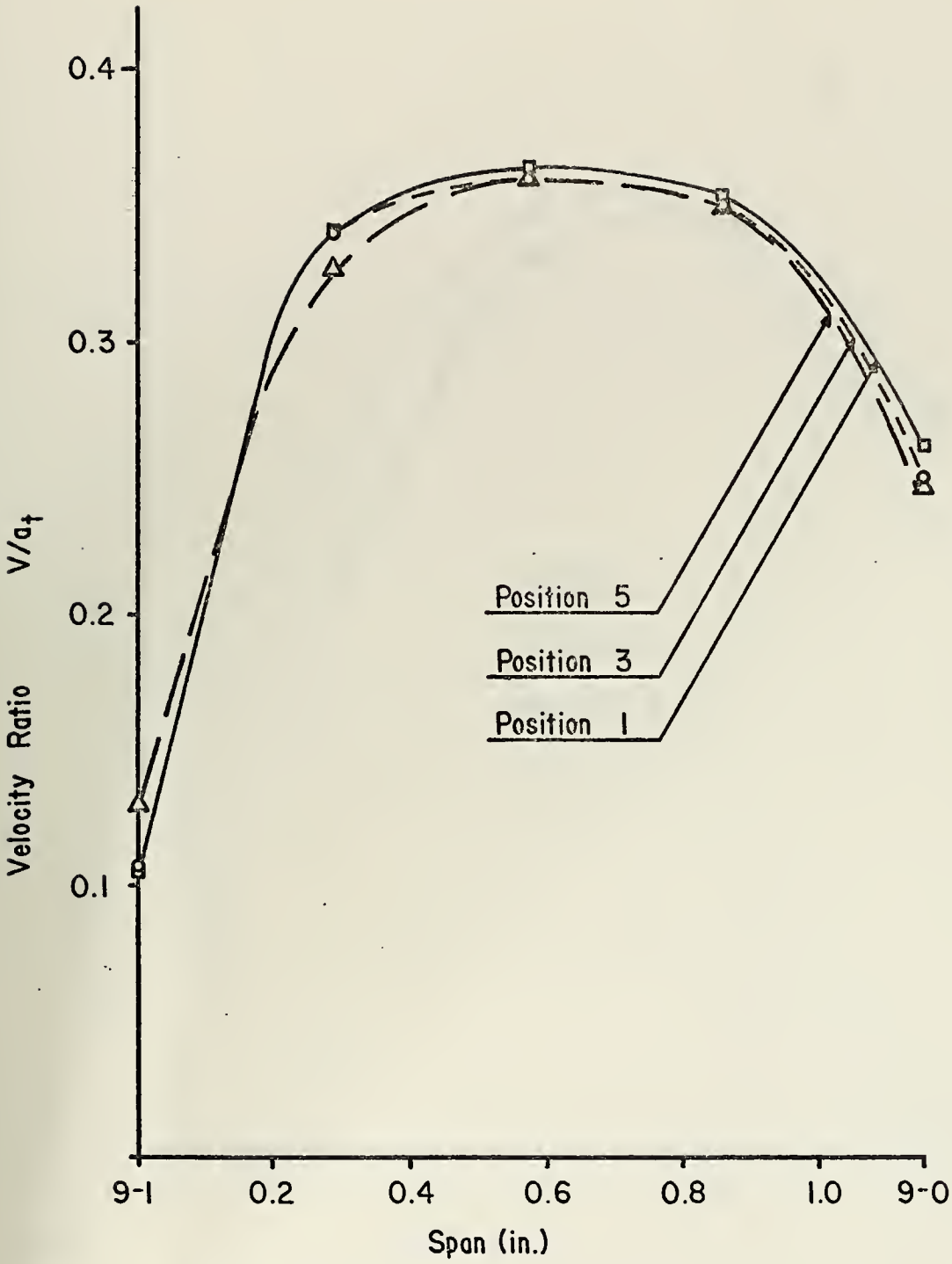

Figure 13 Velocity Ratio versus Span at Station 9 (coarse)

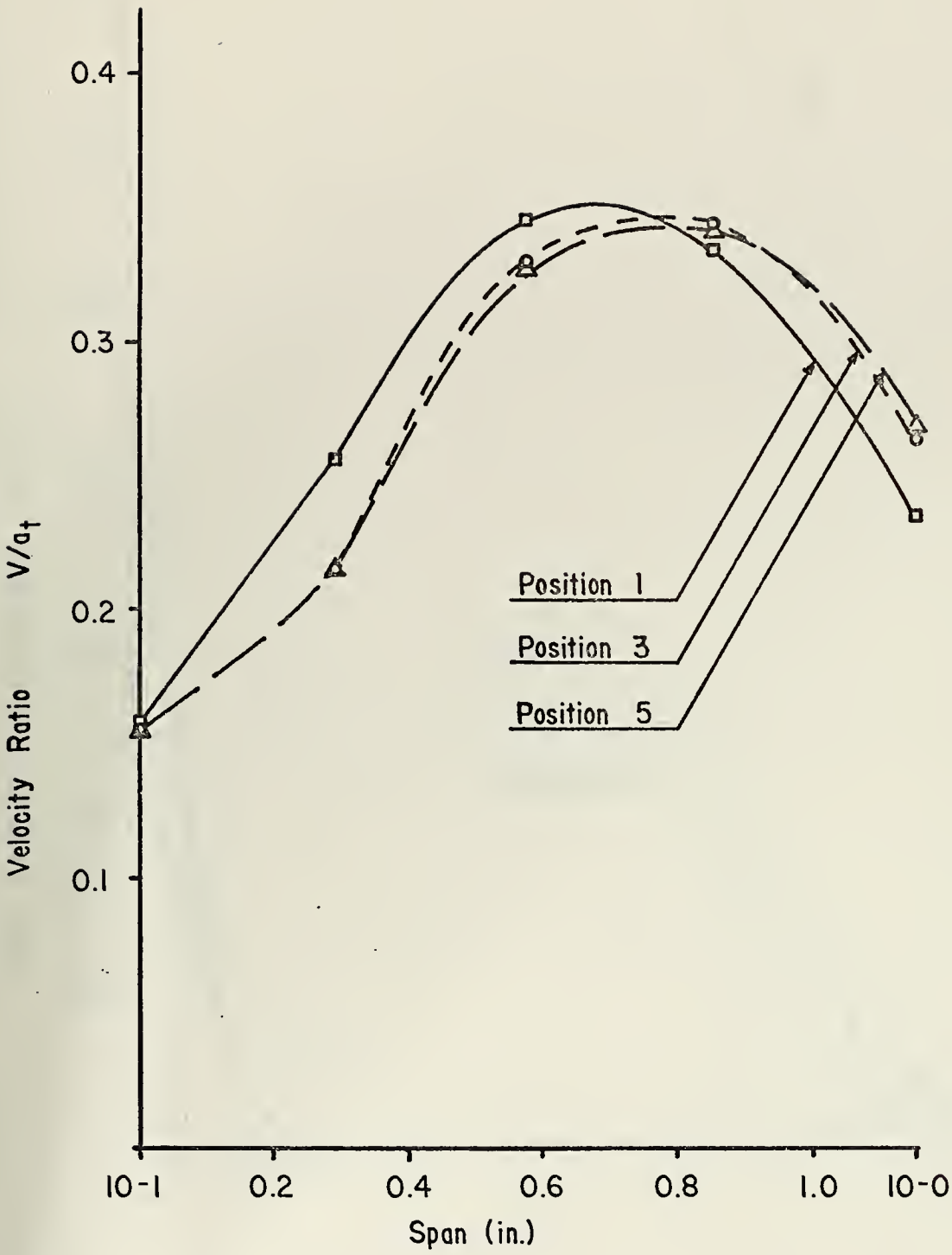

Figure 14 Velocity Ratio versus Span at Station 10 (coarse)

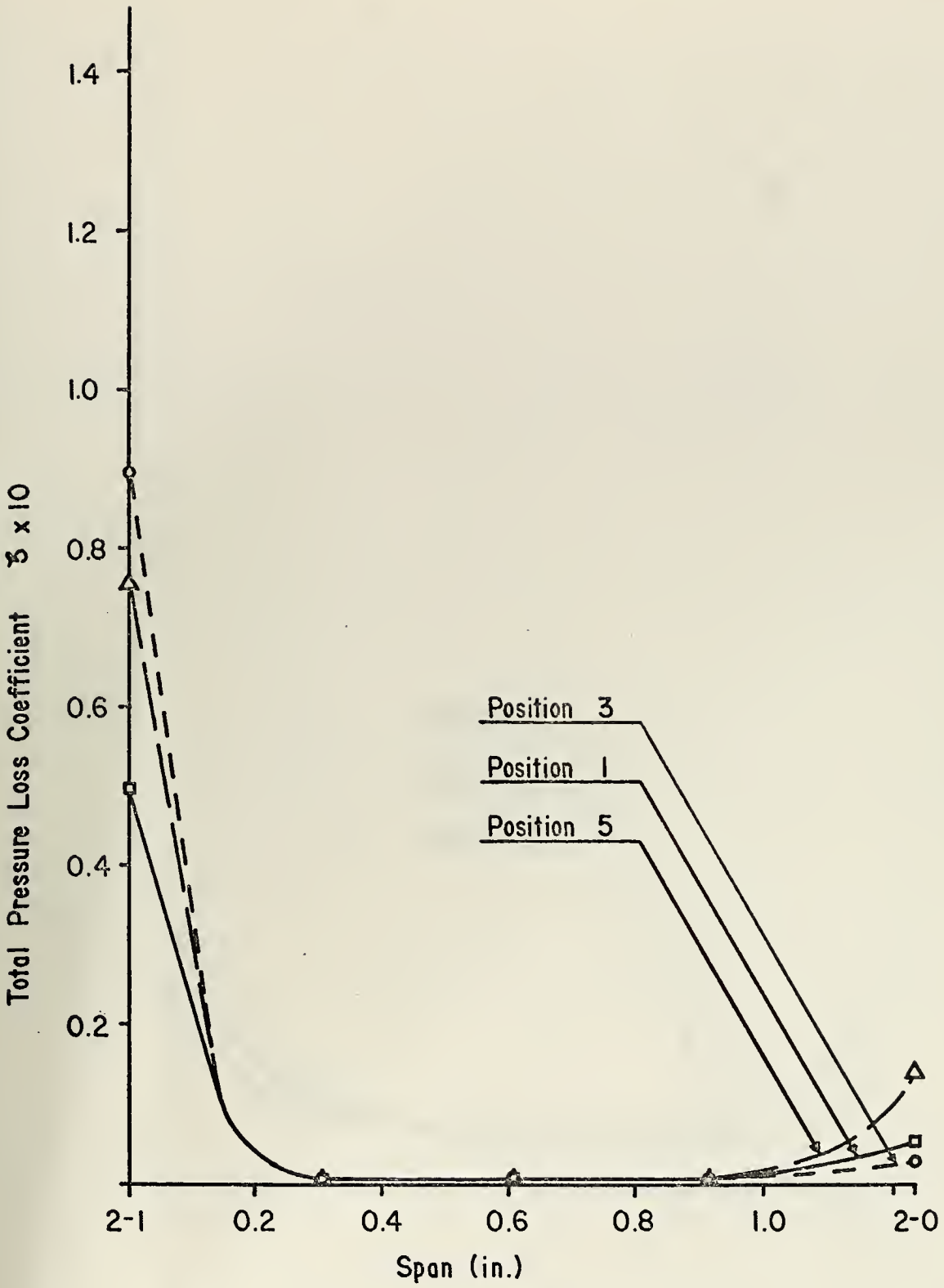

Figure 15 Total Pressure Loss Coefficient versus Span at Station 2 (coarse)

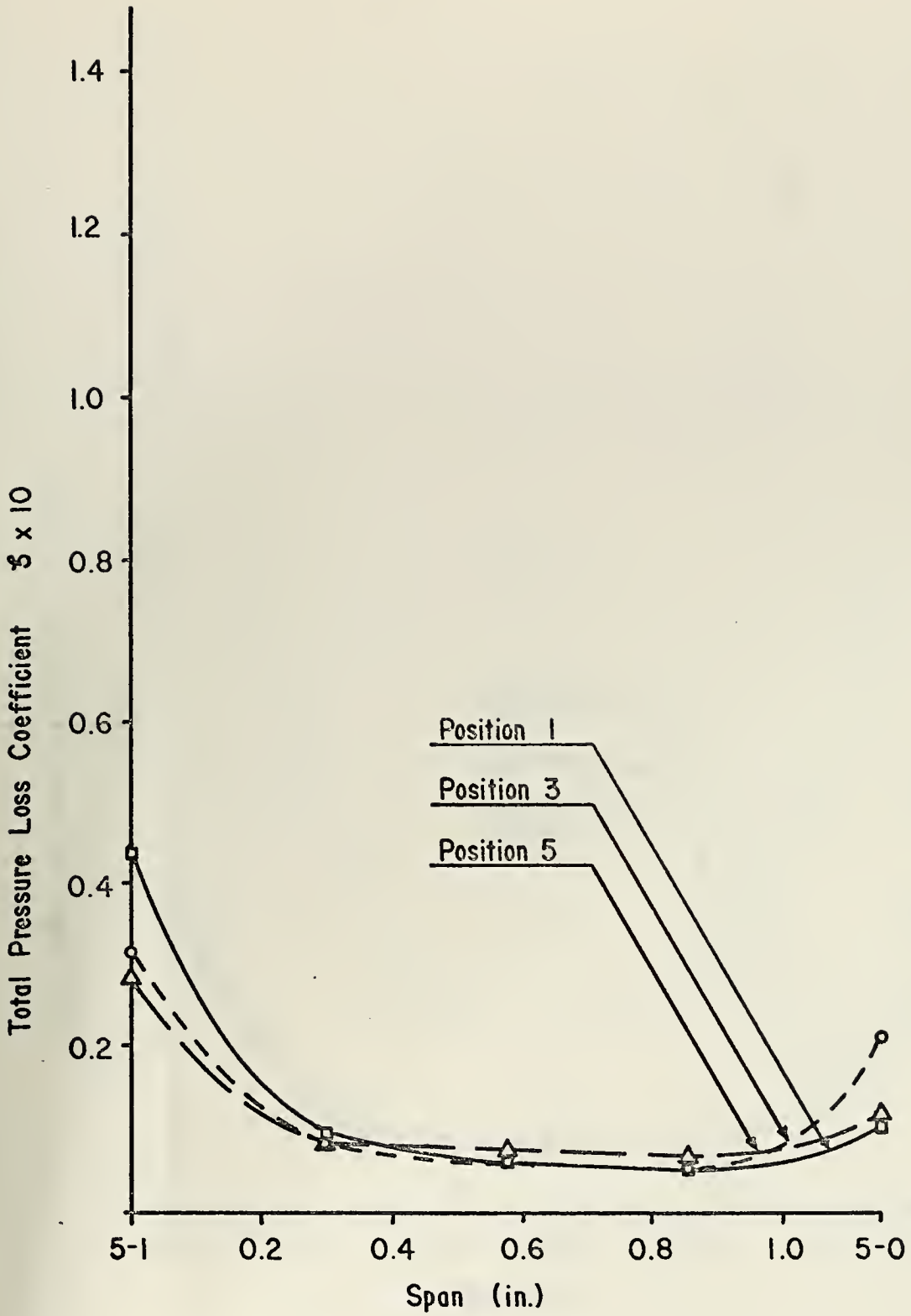

Figure 16 Total Pressure Loss Coefficient versus Span at Station 5 (coarse)

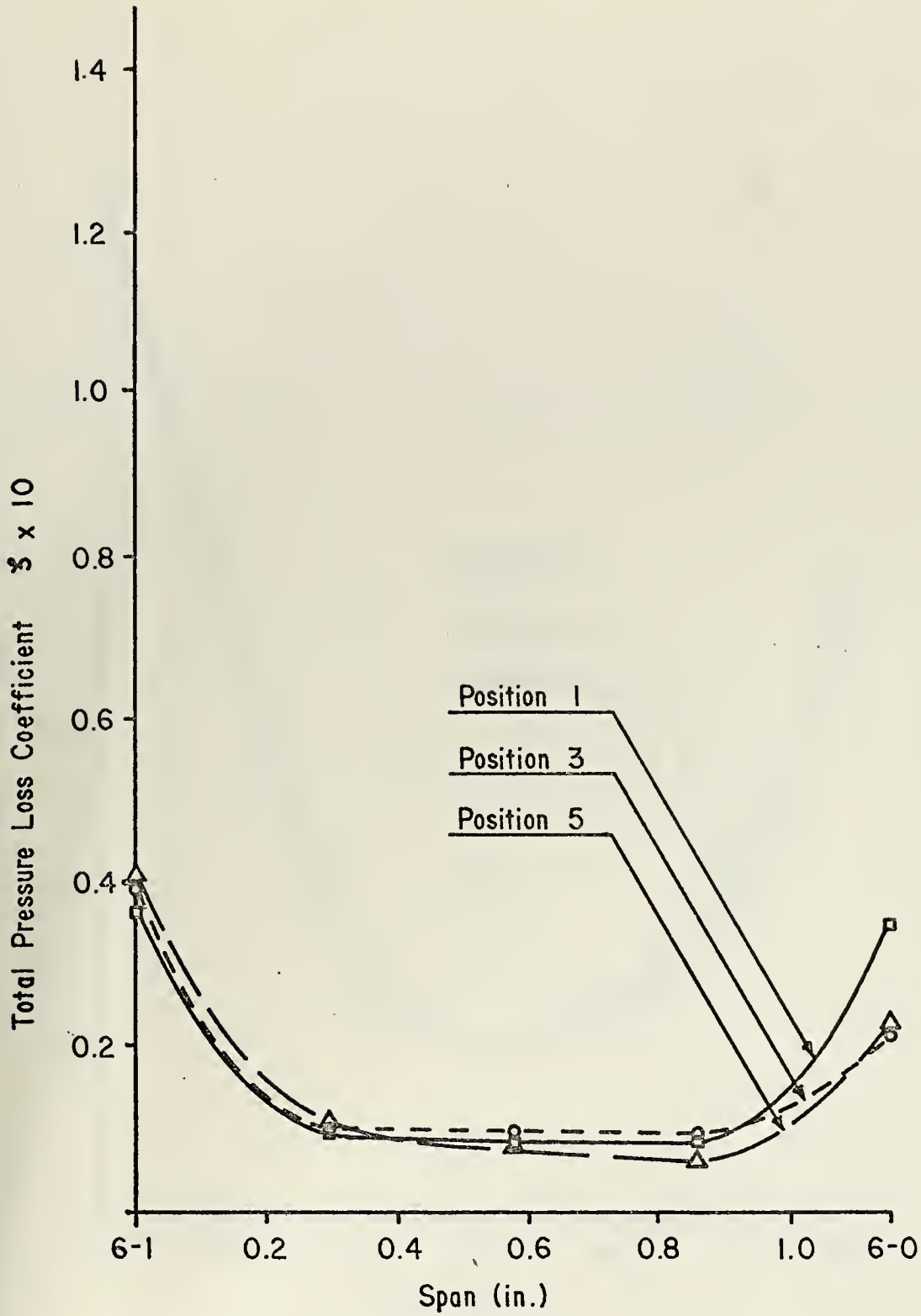

Figure 17 Total Pressure Loss Coefficient versus Span at Station 6 (coarse)

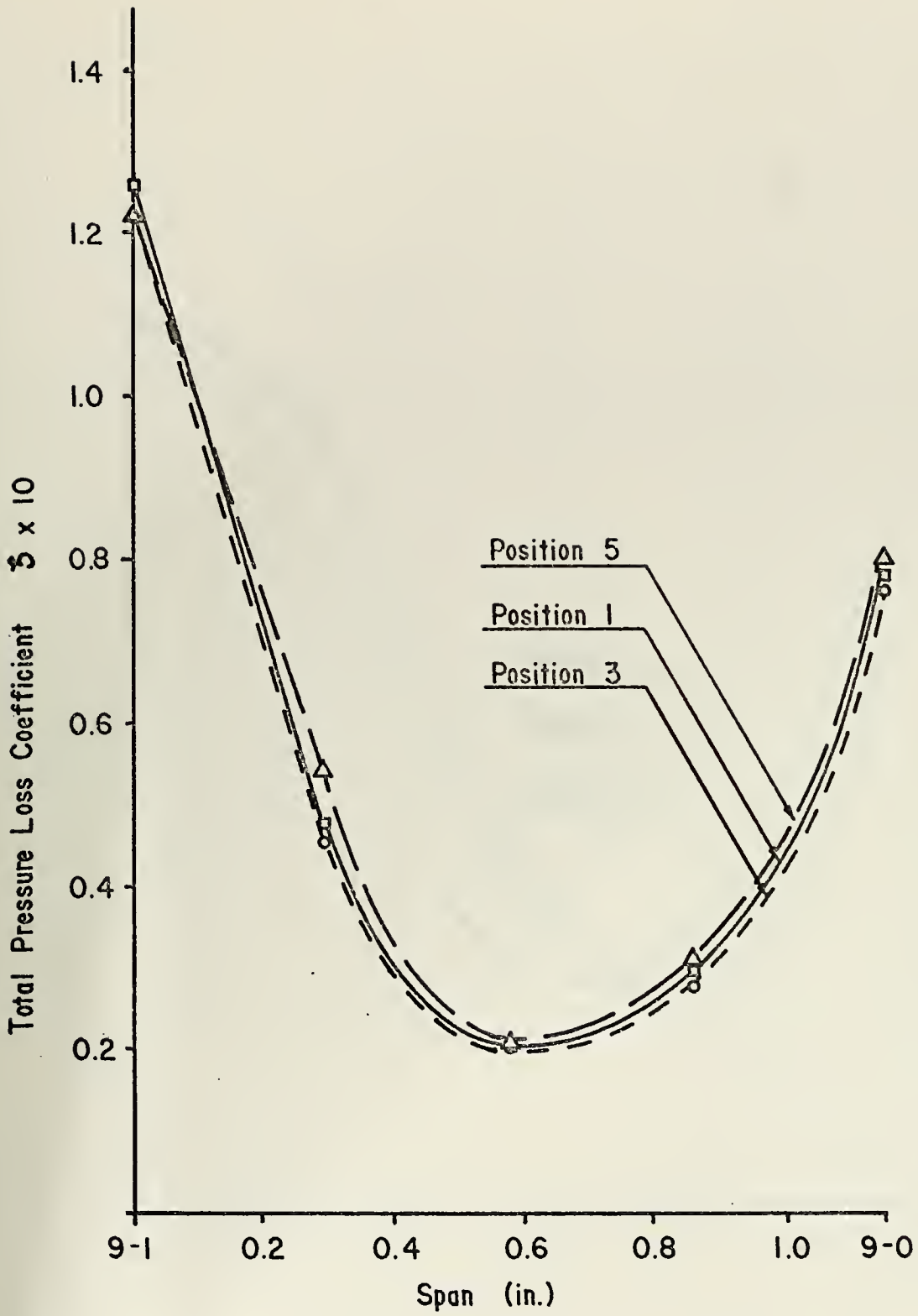

Figure 18 Total Pressure Loss Coefficient versus Span at Station 9 (coarse)

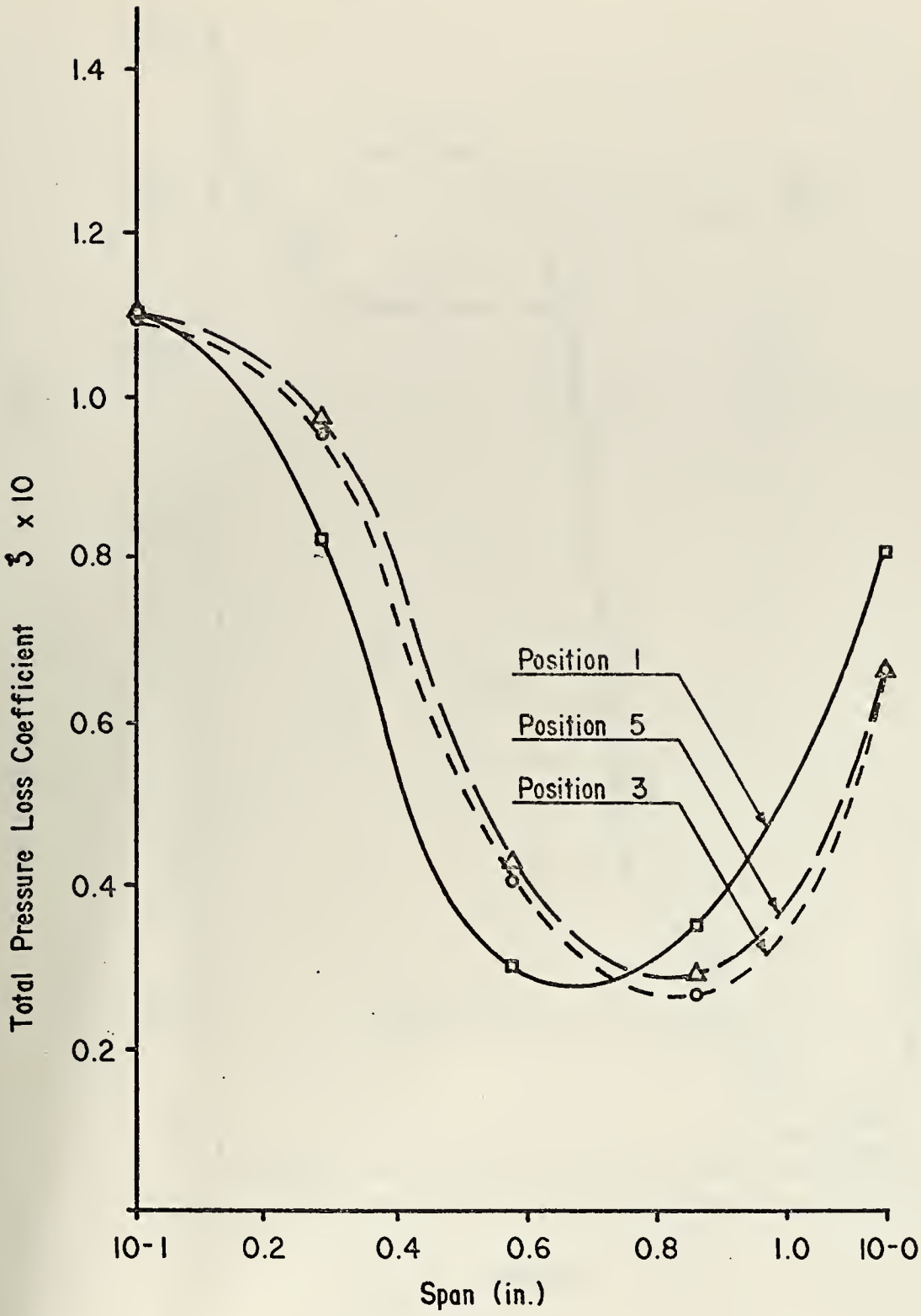

Figure 19 Total Pressure Loss Coefficient versus Span at Station 10 (coarse)

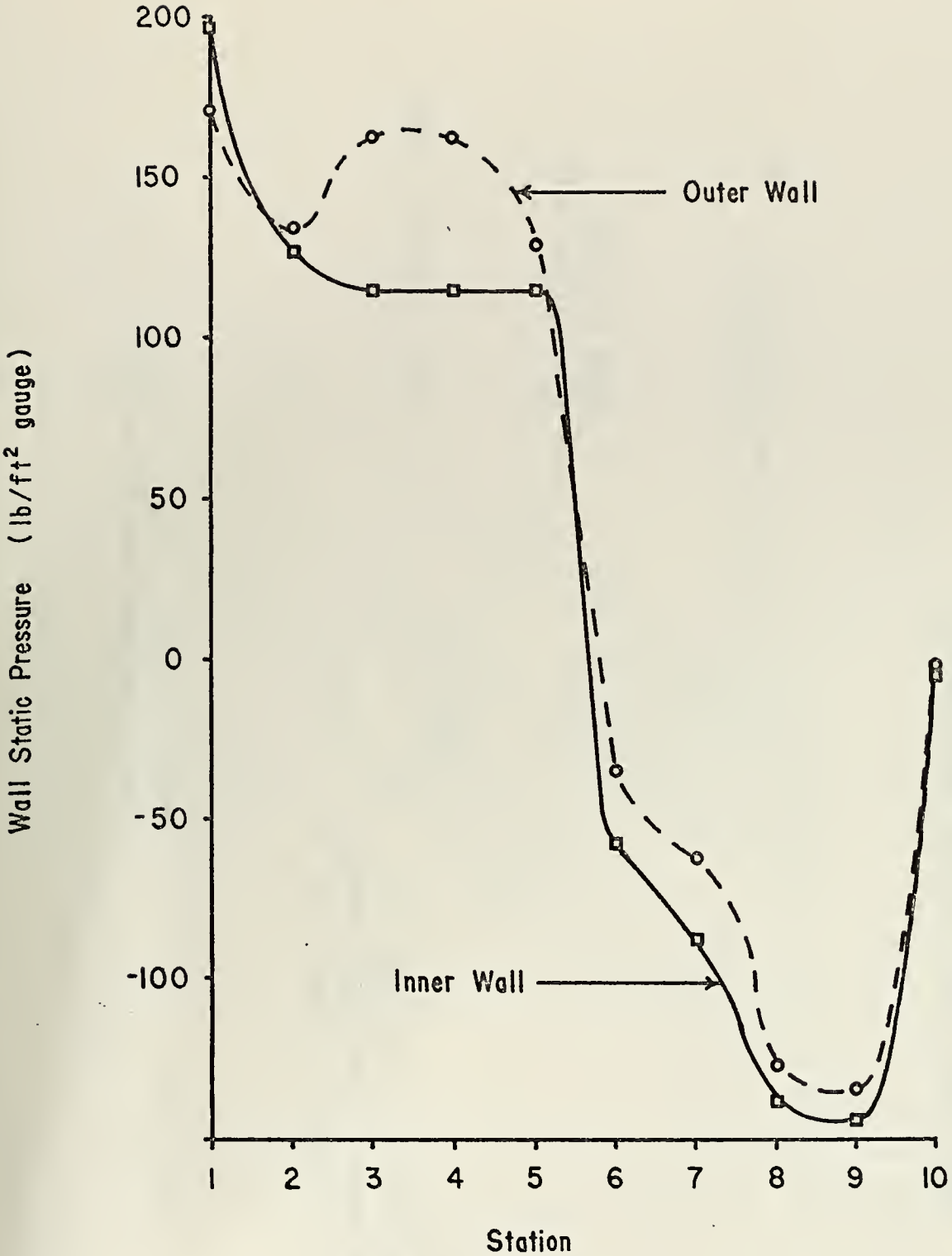

Figure 20 Static Pressure Distribution

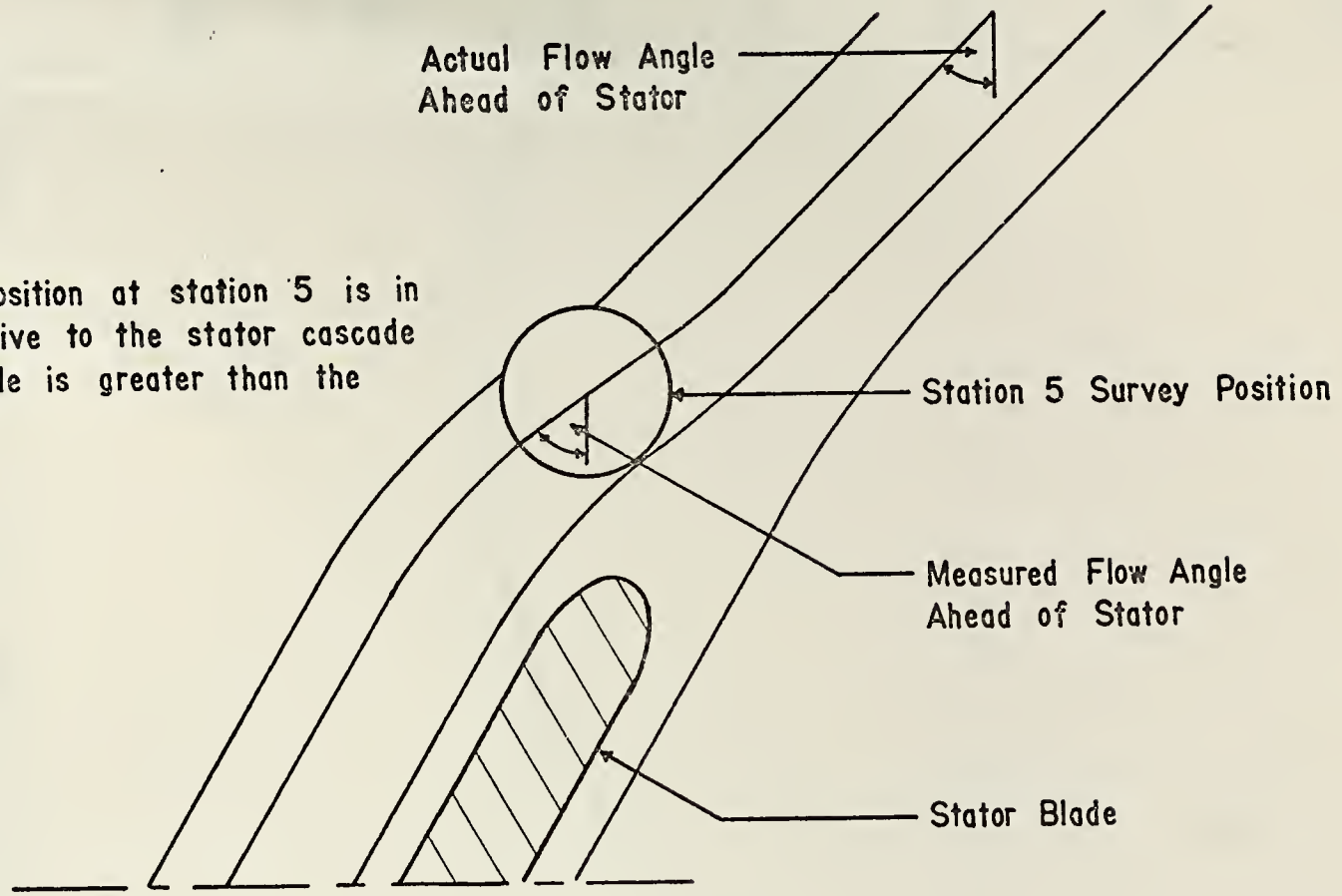

Figure 21 Flow Angle Measurement Discrepancy

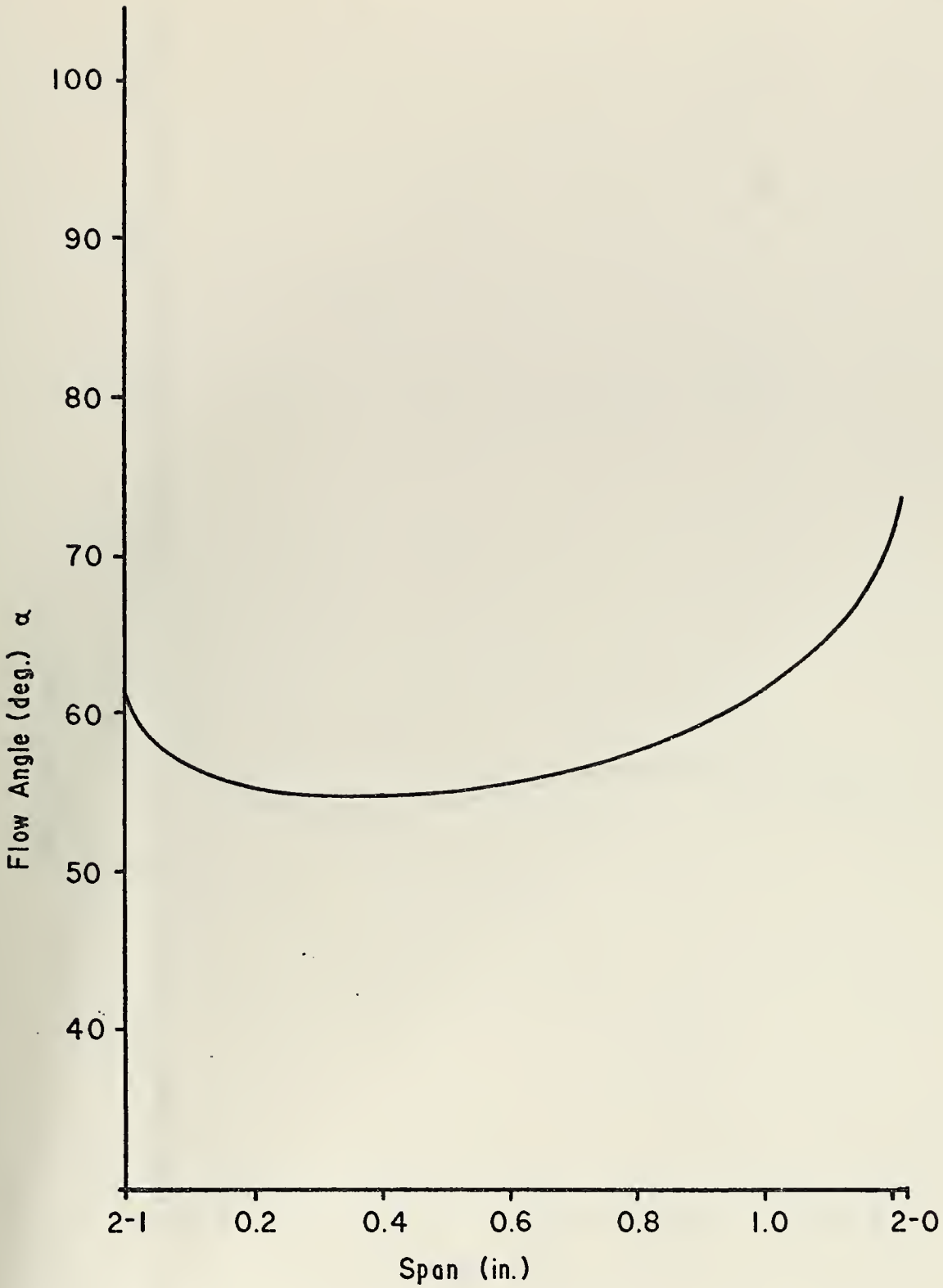

Figure 22 Flow Angle versus Span at Station 2

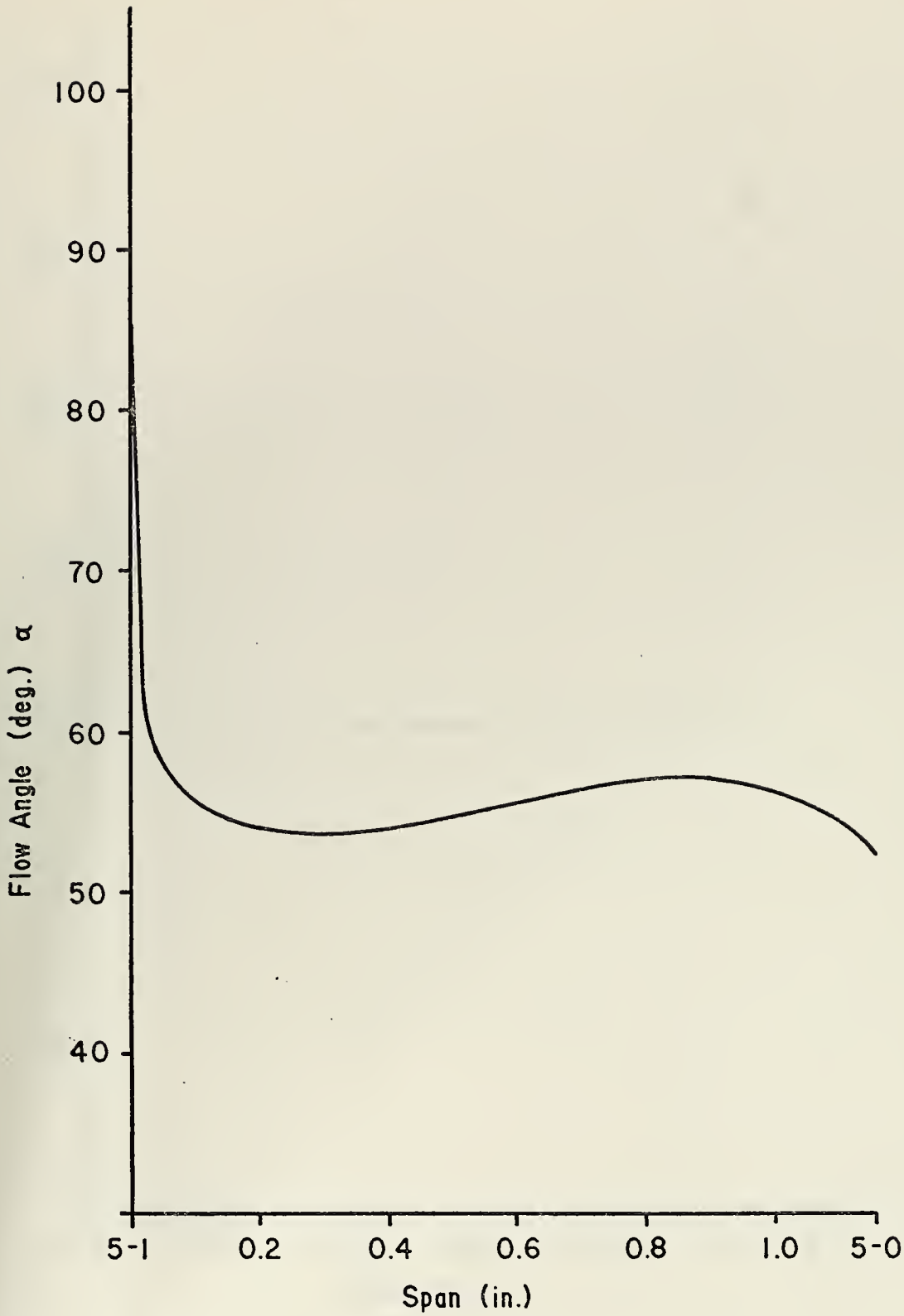

Figure 23 Flow Angle versus Span at Station 5

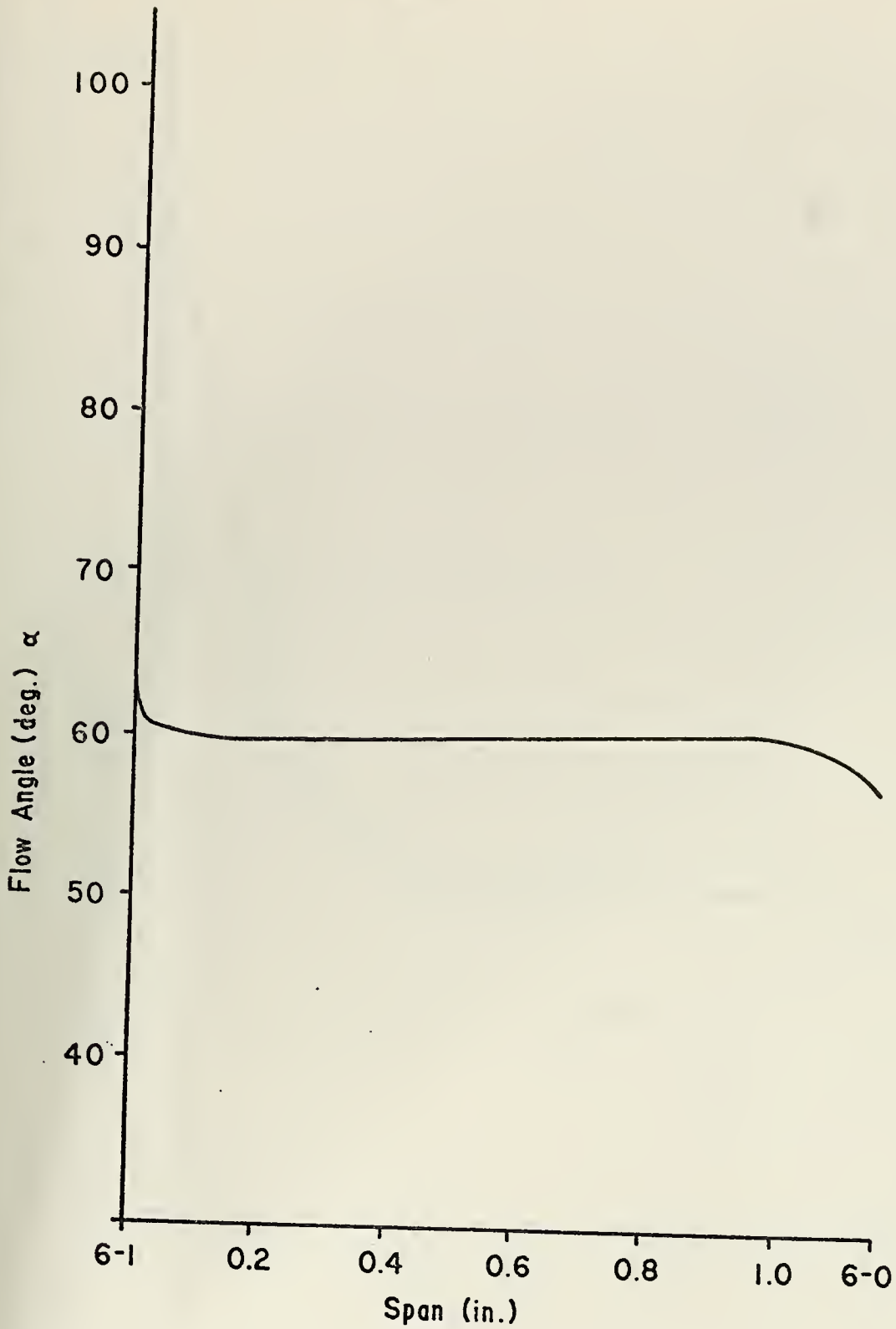

Figure 24 Flow Angle versus Span at Station 6

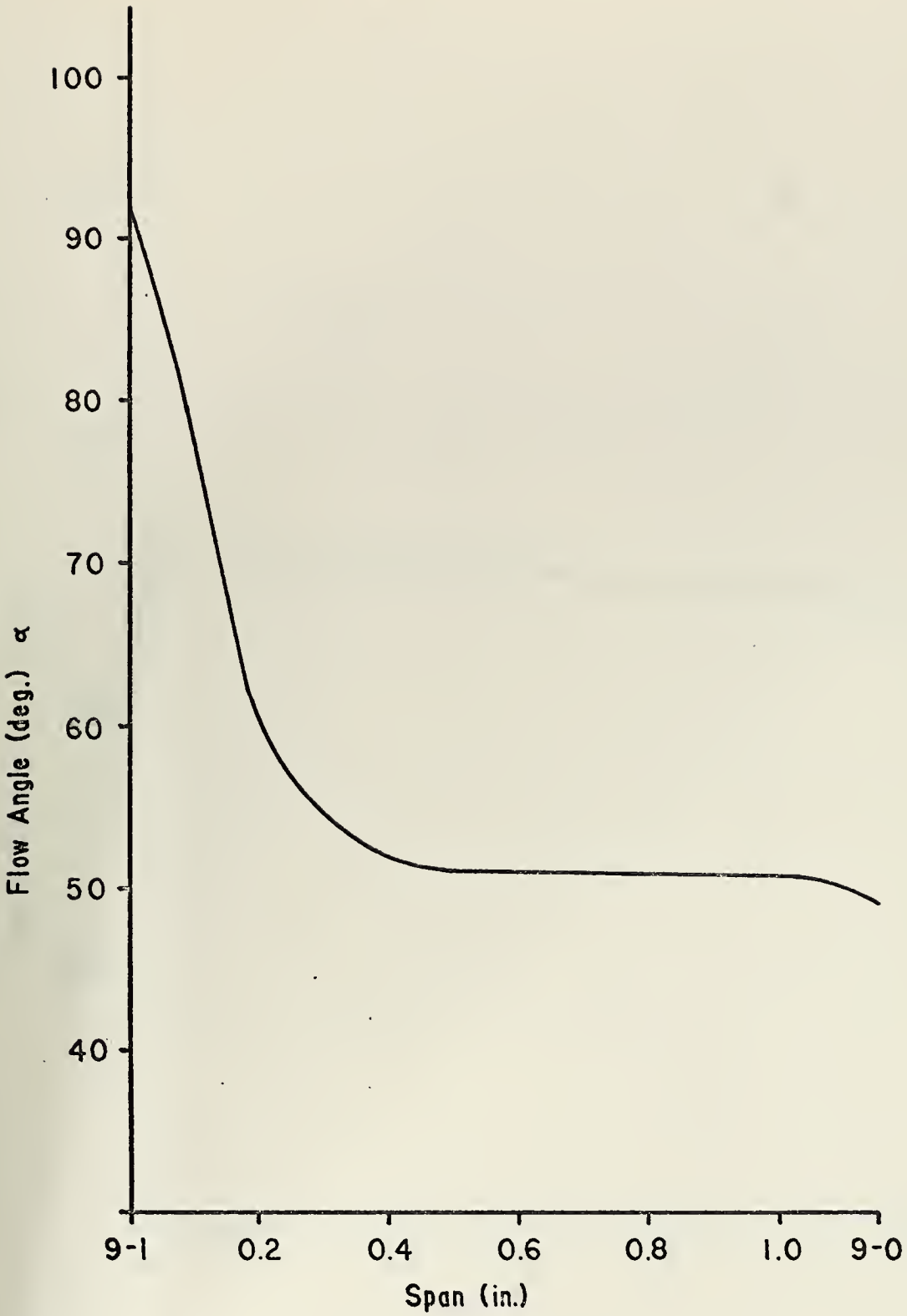

Figure 25 Flow Angle versus Span at Station 9

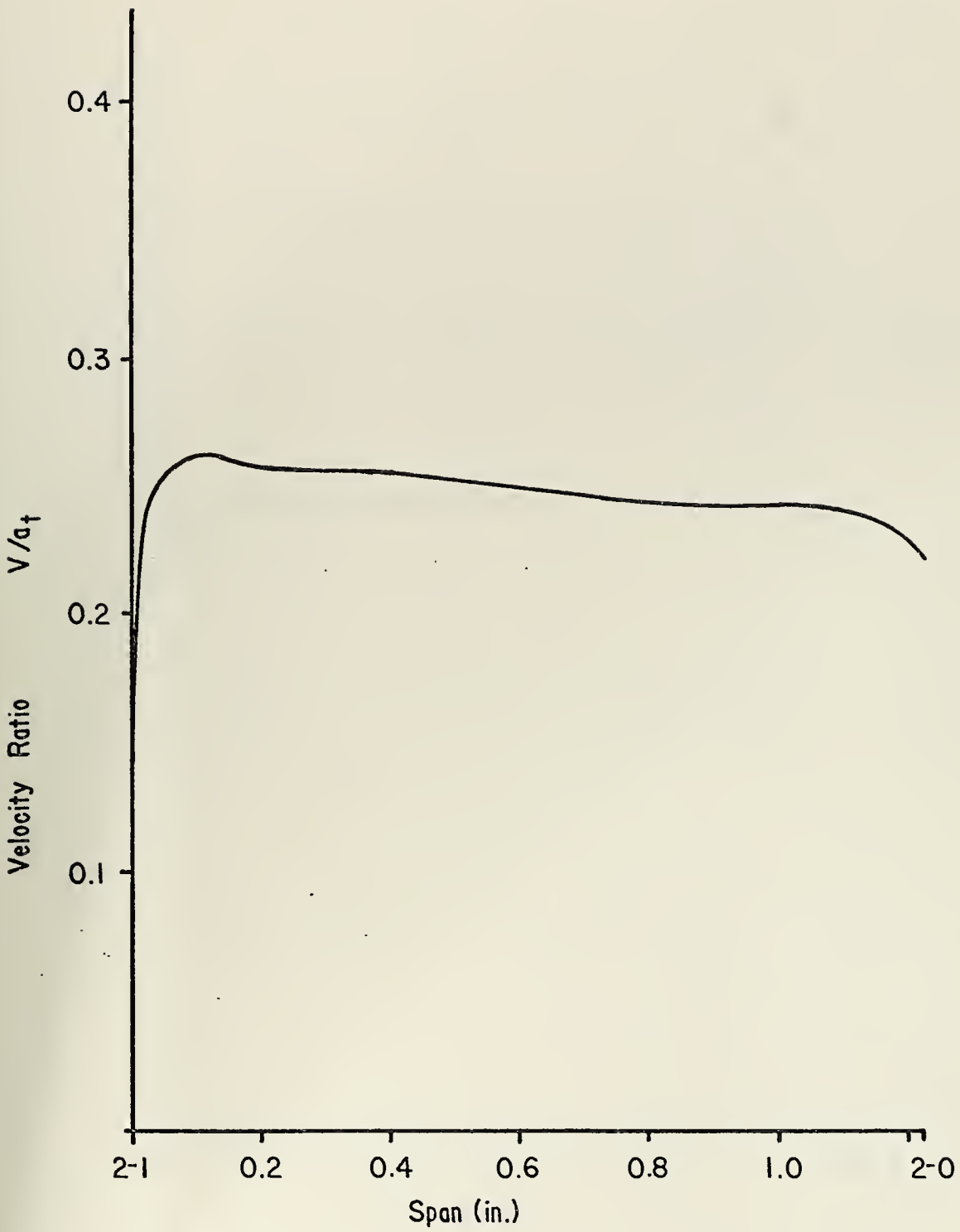

Figure 26 Velocity Ratio versus Span at Station 2

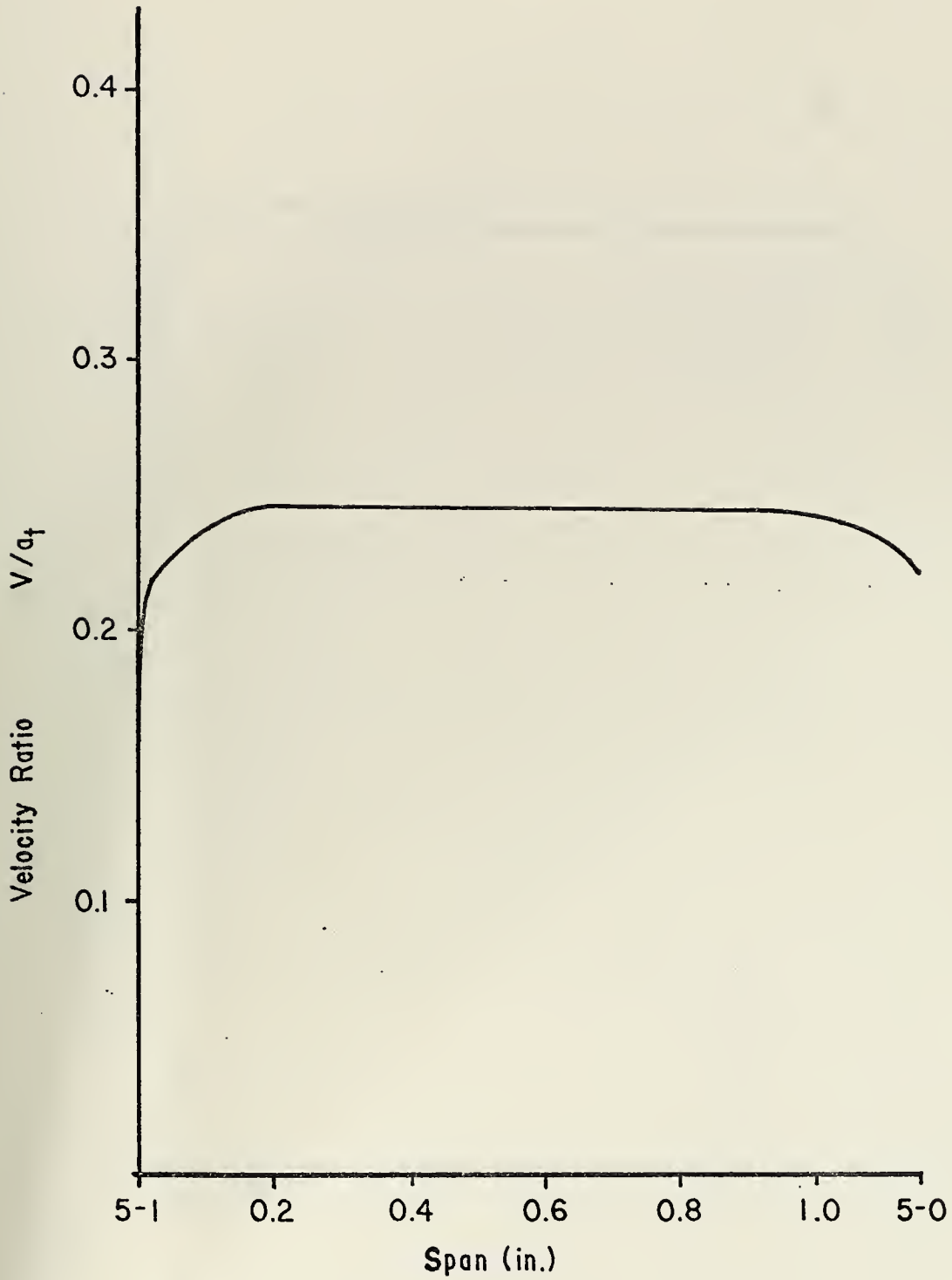

Figure 27 Velocity Ratio versus Span at Station 5

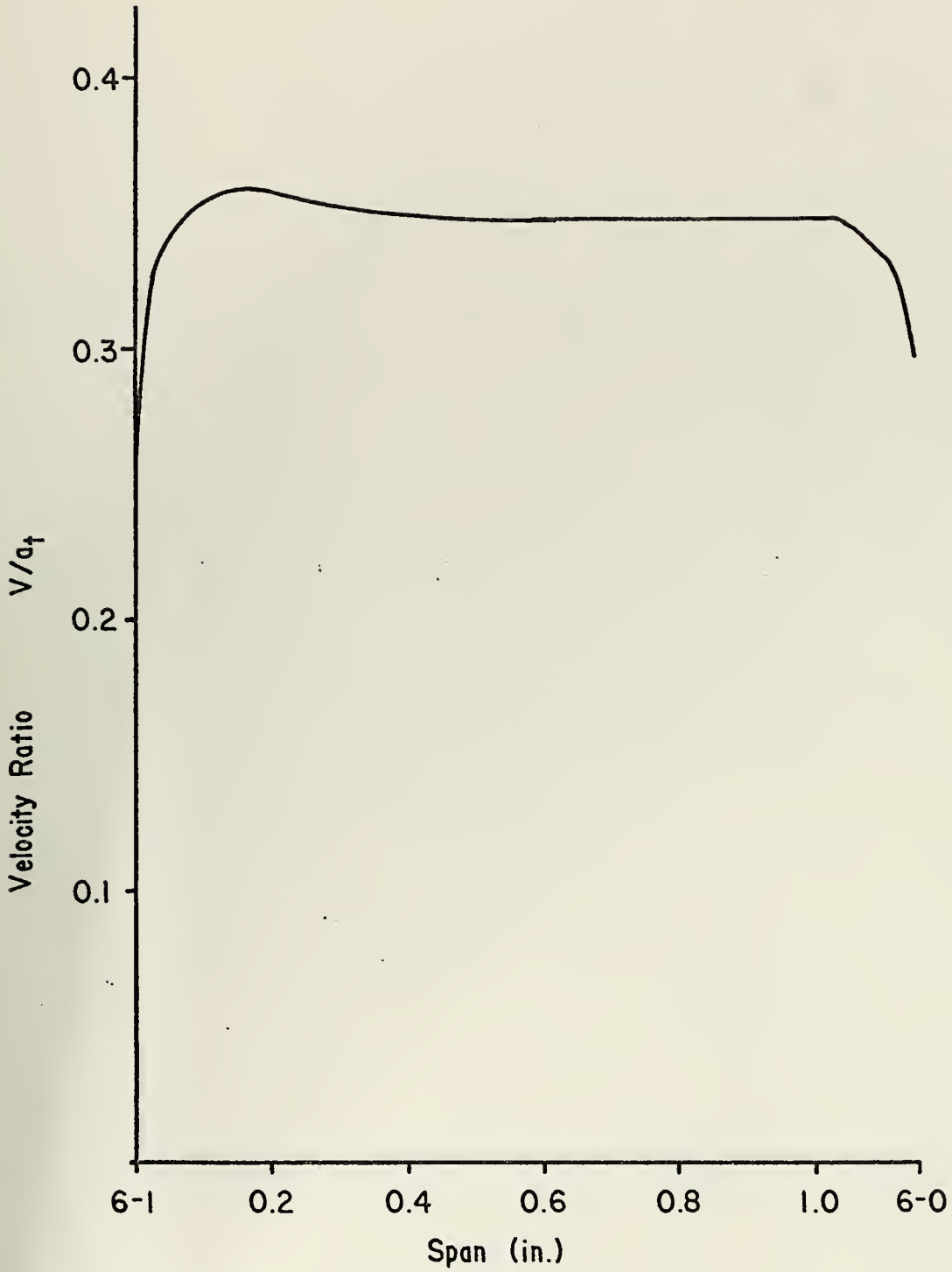

Figure 28 Velocity Ratio versus Span at Station 6

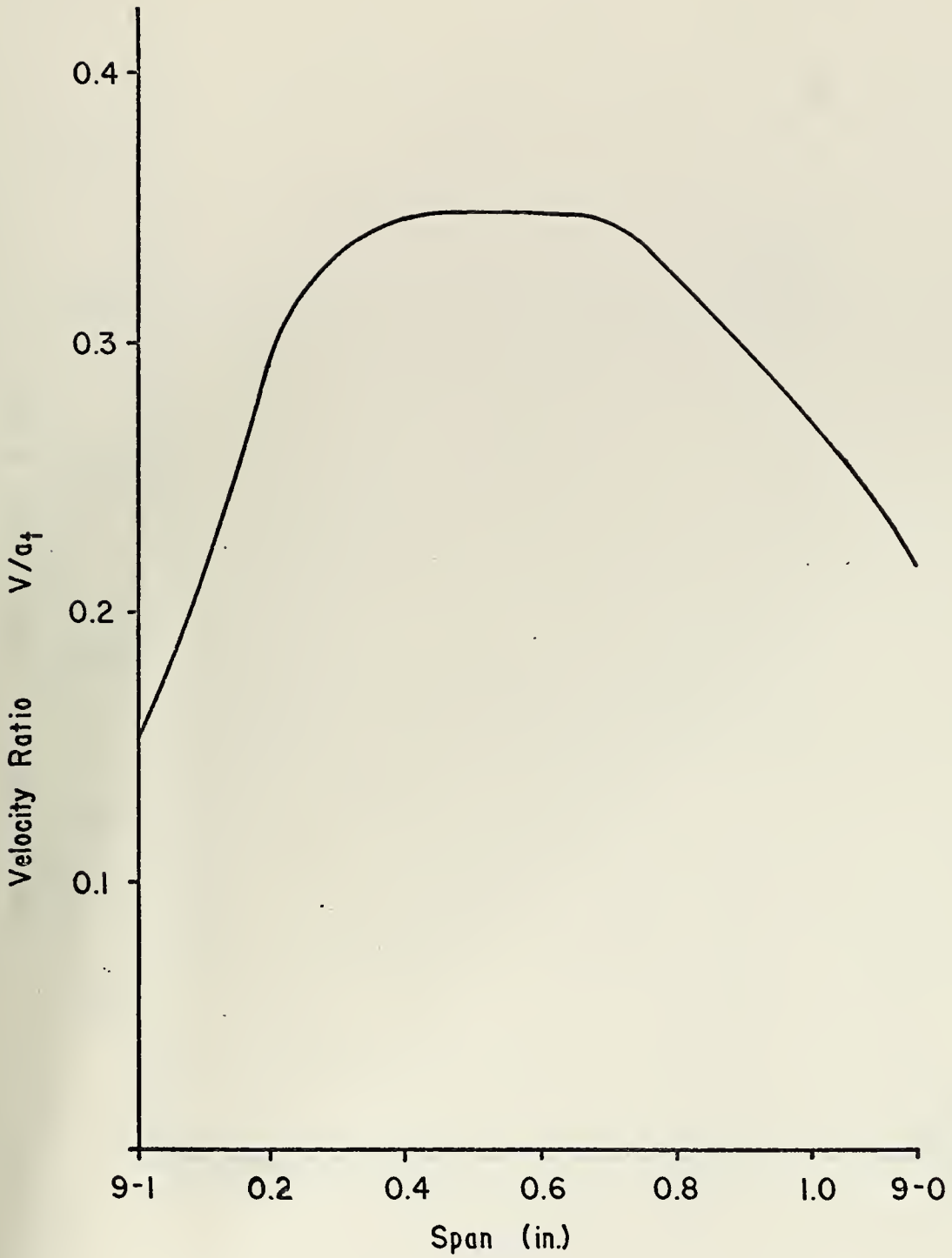

Figure 29 Velocity Ratio versus Span at Station 9

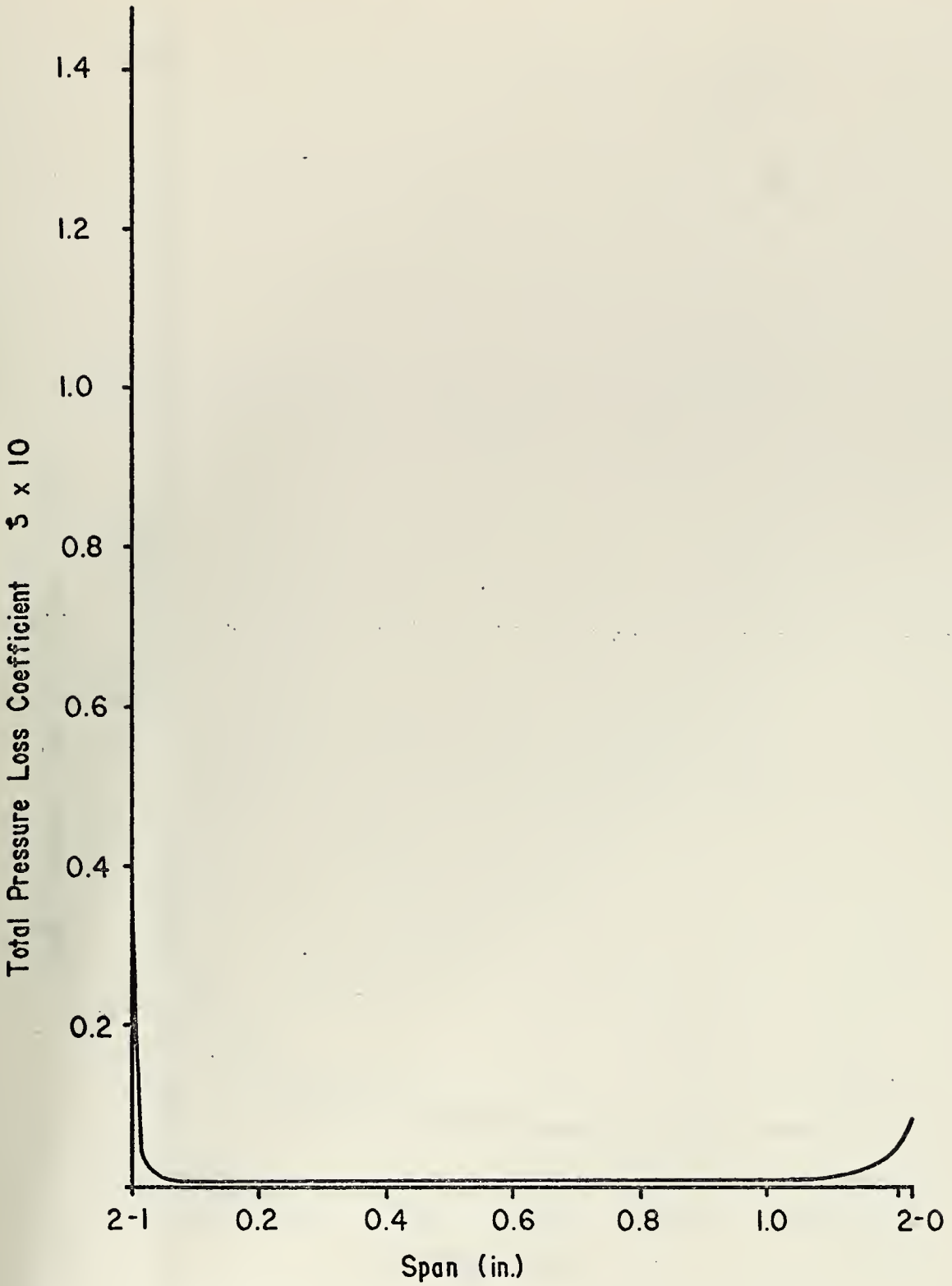

Figure 30 Total Pressure Loss Coefficient versus Span at Station 2

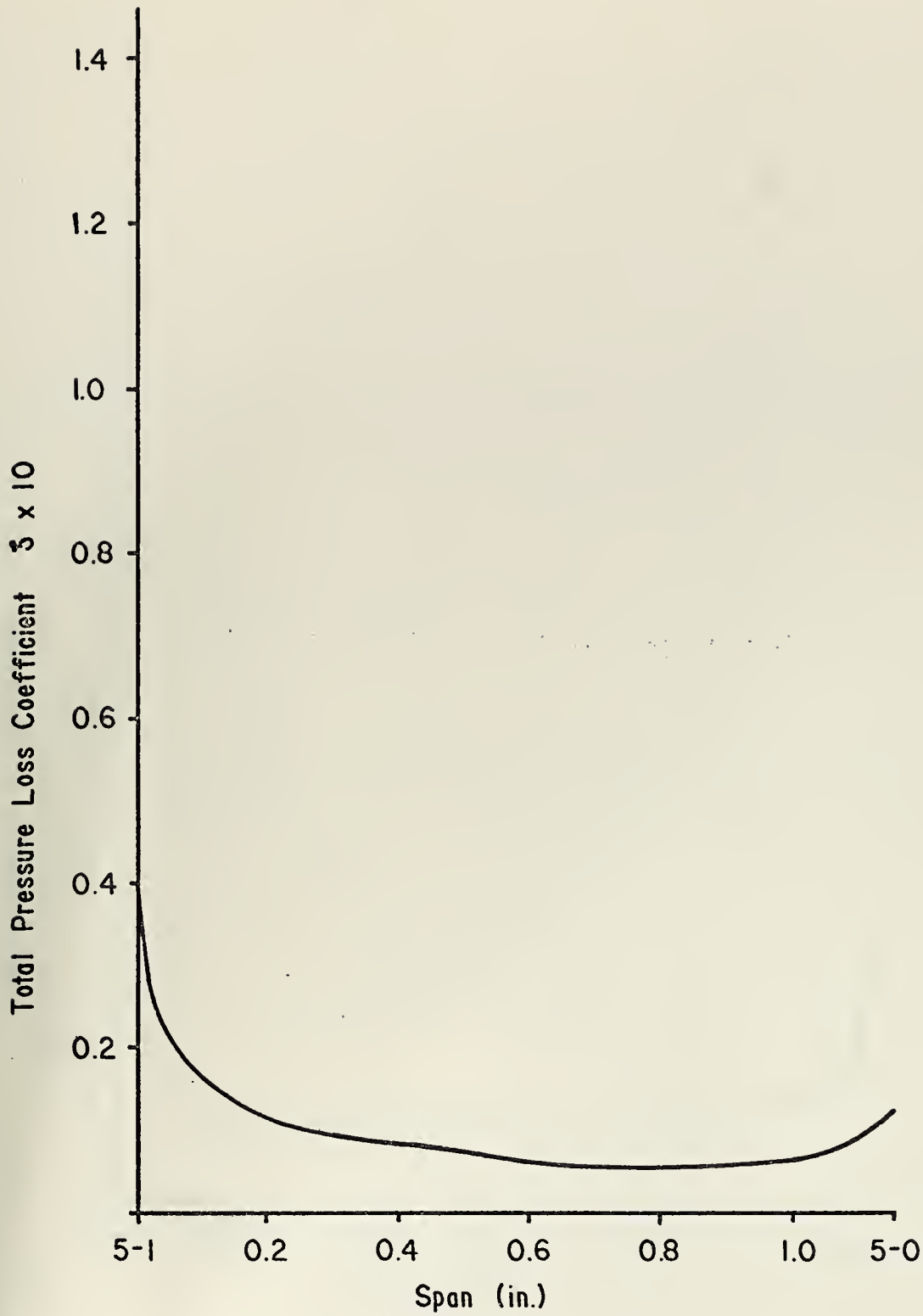

Figure 31 Total Pressure Loss Coefficient versus Span at Station 5

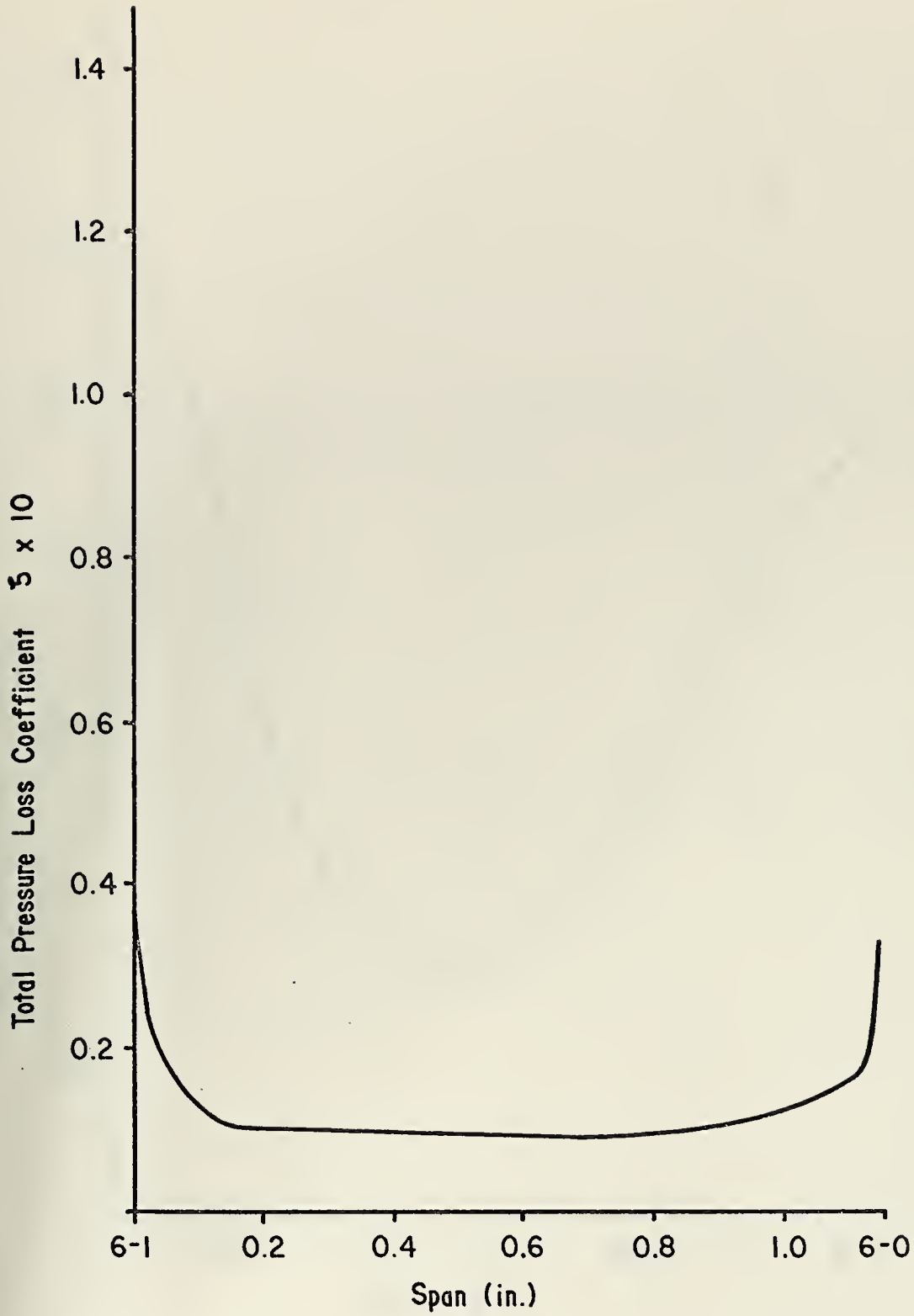

Figure 32 Total Pressure Loss Coefficient versus Span at Station 6

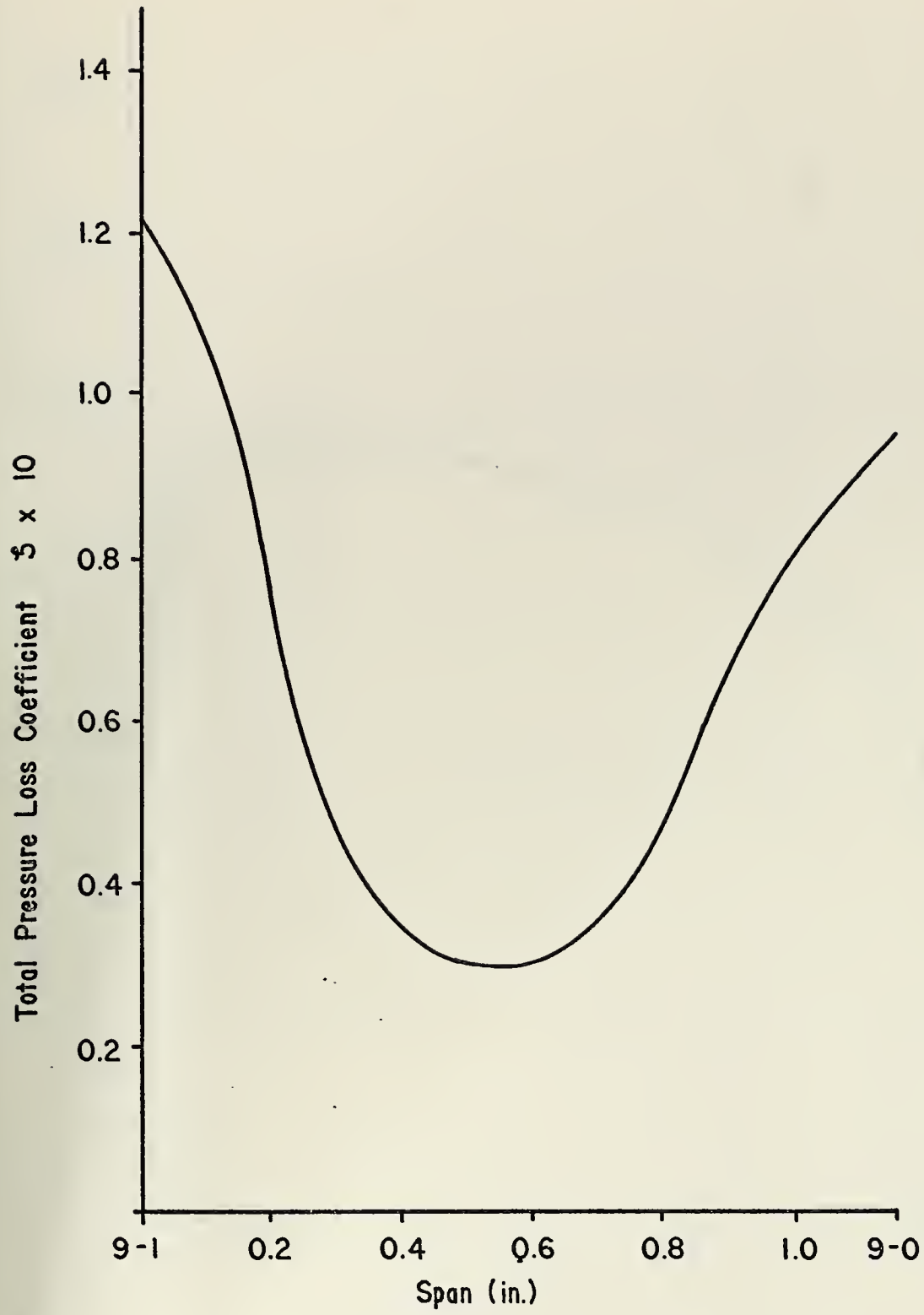

Figure 33 Total Pressure Loss Coefficient versus Span at Station 9

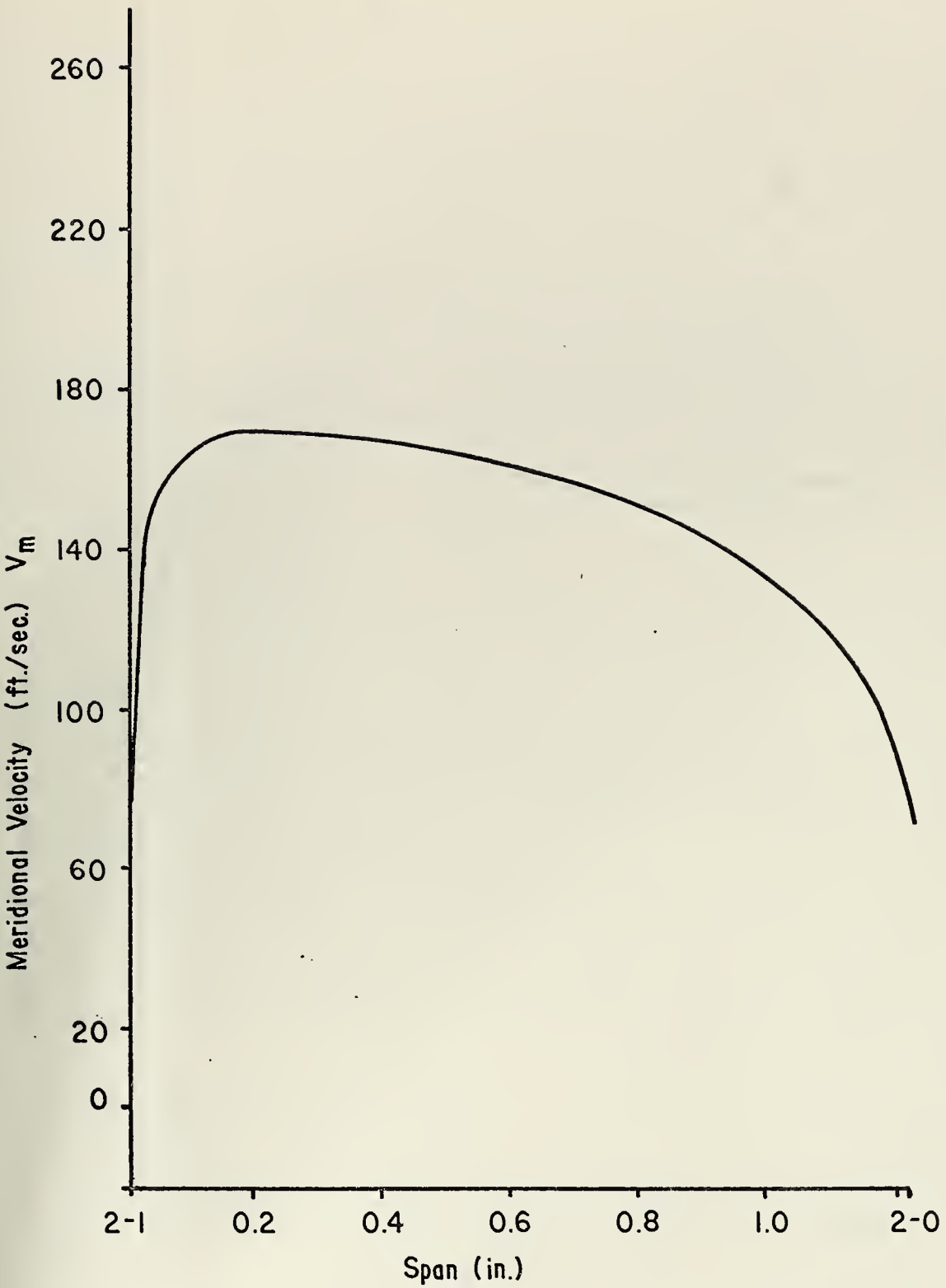

Figure 34 Meridional Velocity versus Span at Station 2

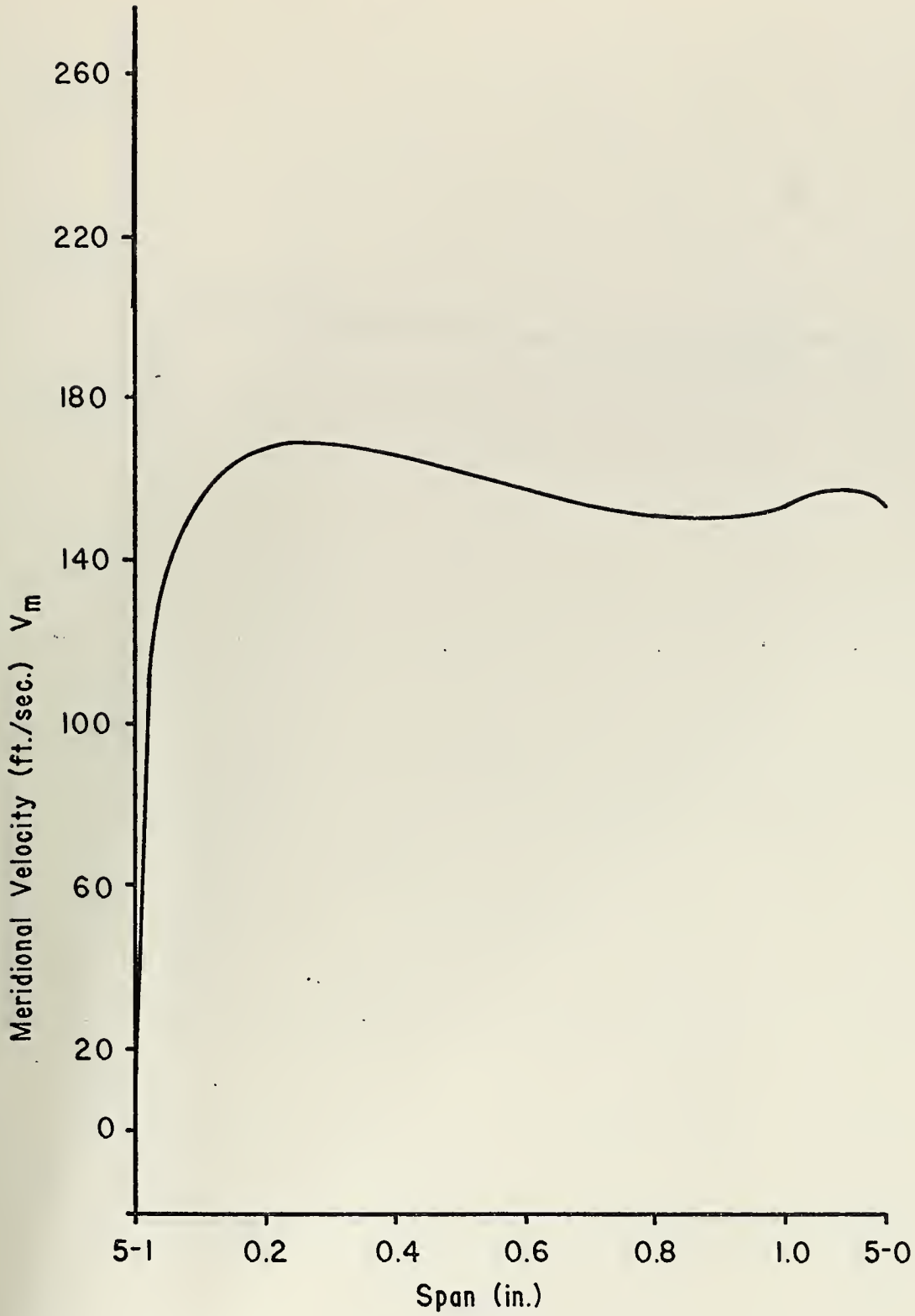

Figure 35 Meridional Velocity versus Span at Station 5

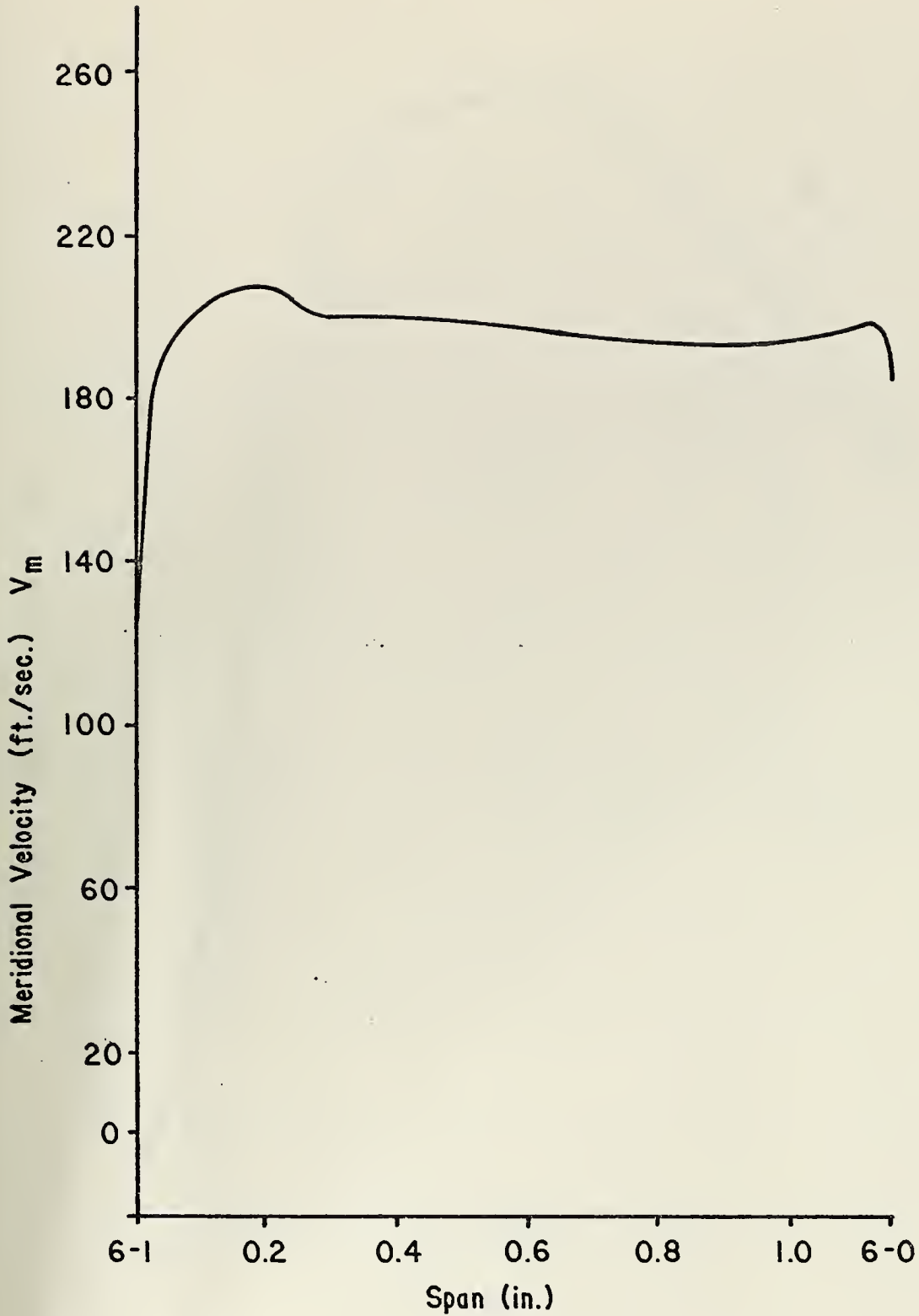

Figure 36 Meridional Velocity versus Span at Station 6

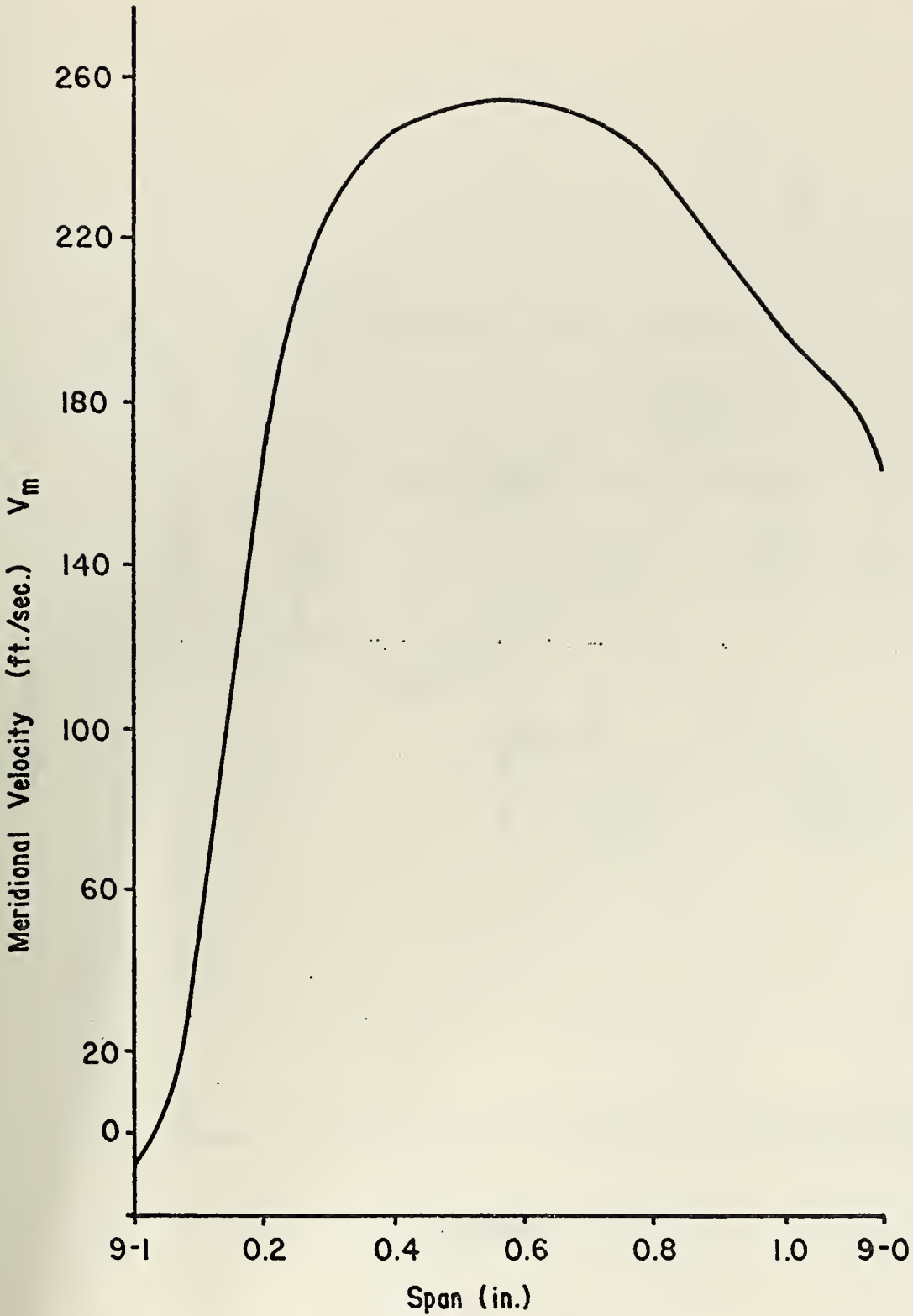

Figure 37 Meridional Velocity versus Span at Station 9

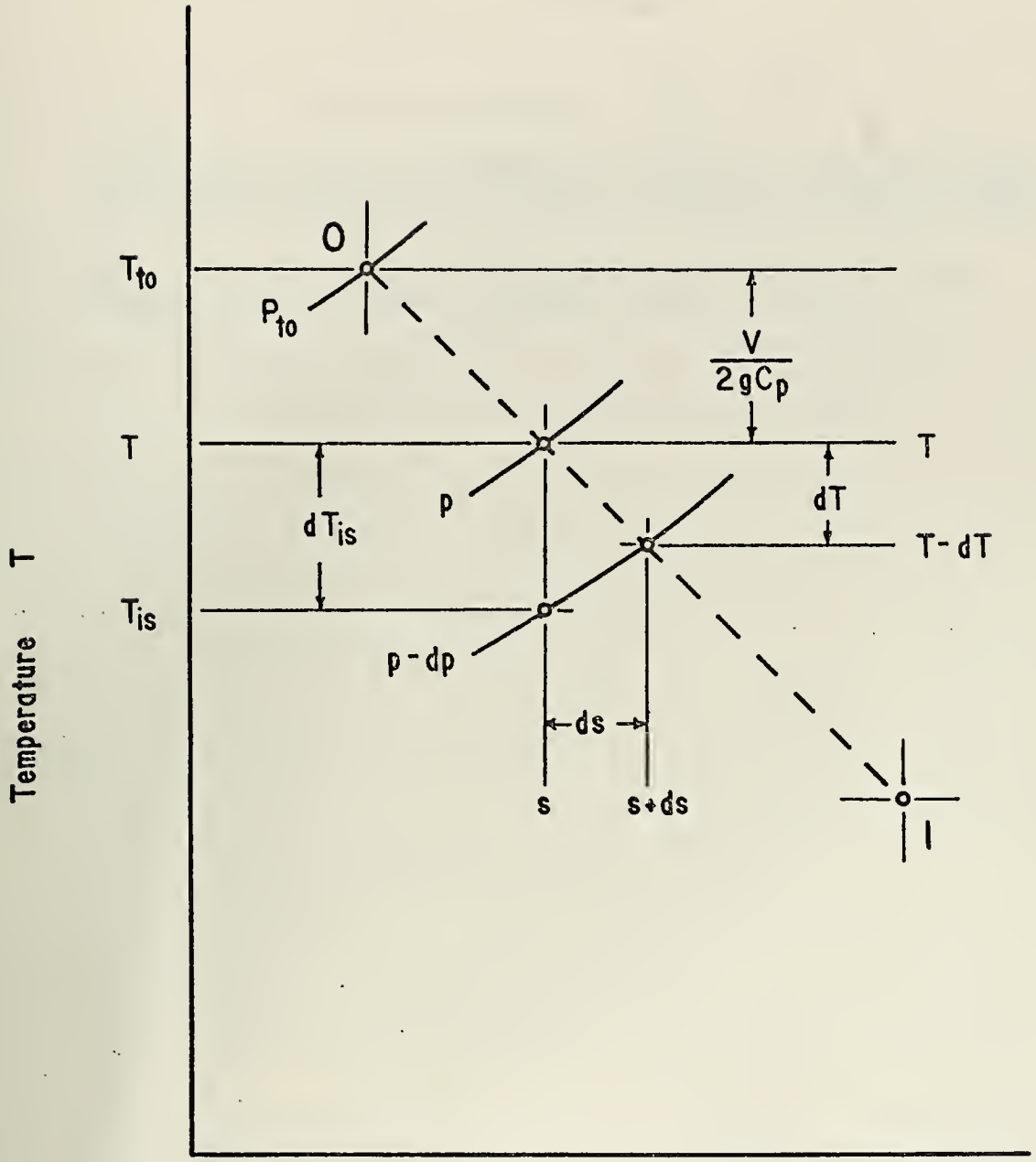

Figure 38 Temperature versus Entropy for an Arbitrary Process

LIST OF REFERENCES

1. Vavra, M. H., Energy Absorber, April 1970.

2. Rolek, L. S. Jr., Performance Analysis of a Turbo-Type Energy Absorber for an Aircraft Carrier Arresting Gear, M.S. Thesis, Naval Postgraduate School, Monterey, 1971.

3. Vavra, M. H., Aero-Thermodynamics and Flow in Turbo-machines, John Wiley and Sons, 1960.

INITIAL DISTRIBUTION LIST

		No. Copies
1.	Defense Documentation Center Cameron Station Alexandria, Virginia 22314	2
2.	Library, Code 0212 Naval Postgraduate School Monterey, California 93940	2
3.	Superintendent, Code 00 Naval Postgraduate School Monterey, California 93940	1
4.	Provost, Code 02 Naval Postgraduate School Monterey, California 93940	1
5.	Dean of Research Administration, Code 023 Naval Postgraduate School Monterey, California 93940	1
6.	Chairman, Department of Aeronautics, Code 57 Naval Postgraduate School Monterey, California 93940	1
7.	Curricular Officer Aeronautical Engineering Program, Code 31 Naval Postgraduate School Monterey, California 93940	1
8.	Turbo-Propulsion Laboratory Department of Aeronautics Naval Postgraduate School Monterey, California 93940	5
9.	Commanding Officer Naval Air Systems Command Navy Department Washington, D. C. 20360	1
10.	Commandin g Officer Naval Air Engineering Center Philadelphia, Pennsylvania 19112	1

11.	Mr. W. E. Gallant, NE-712 Naval Air Engineering Center Philadelphia, Pennsylvania 19112	2
12.	Rear Admiral Rupert S. Miller, USN Asst. Commander for Research and Technology Naval Air Systems Command Navy Department Washington, D. C. 20360	1
13.	Dr. H. J. Mueller Research Administrator, Code 310A Naval Air Systems Command Navy Department Washington, D. C. 20360	1
14.	Mr. Karl H. Guttman, Code 330C Naval Air Systems Command Navy Department Washington, D. C. 20360	1
15.	Rear Admiral C. O. Holmquist, USN Chief of Naval Research Office of Naval Research Arlington, Virginia 22218	1
16.	Commanding Officer Naval Air Propulsion Test Center Attention: Mr. E. Stawski Trenton, New Jersey 08628	1
17.	Mr. Eric Lister R. & T. Division Naval Air Propulsion Test Center Trenton, New Jersey 08628	1
18.	Professor M. H. Vavra, Code 57Va Department of Aeronautics Naval Postgraduate School Monterey, California 93940	1
19.	Lt. T. A. Morgenfeld USN Fighter Squadron 191 FPO San Francisco, California 96601	1

Security Classification

DOCUMENT CONTROL DATA - R & D

(Security classification of title, body of abstract and indexing annotation must be entered when the overall report is classified)

ORIGINATING ACTIVITY *(Corporate author)*

Naval Postgraduate School
Monterey, California 93940

2a. REPORT SECURITY CLASSIFICATION

Unclassified

2b. GROUP

REPORT TITLE

Model Test of a Turbo-Type Energy Absorber for Aircraft Carrier Arresting Gear

DESCRIPTIVE NOTES *(Type of report and inclusive dates)*

Master's Thesis, March 1973

AUTHOR(S) *(First name, middle initial, last name)*

Thomas A. Morgenfeld

REPORT DATE	7a. TOTAL NO. OF PAGES	7b. NO. OF REFS
March 1973	80	3

a. CONTRACT OR GRANT NO.	9a. ORIGINATOR'S REPORT NUMBER(S)
b. PROJECT NO.	
c.	9b. OTHER REPORT NO(S) *(Any other numbers that may be assigned this report)*
d.	

10. DISTRIBUTION STATEMENT

Approved for public release; distribution unlimited.

11. SUPPLEMENTARY NOTES	12. SPONSORING MILITARY ACTIVITY
	Naval Postgraduate School Monterey, California 93940

13. ABSTRACT

Increasing energy absorption requirements are being placed on present day aircraft carrier arresting gear engines. Hydraulic ram type engines have reached the upper limit of their development due to weight and space limitations. A turbo-type energy absorber has been proposed as an alternative. The Naval Air Engineering Center is currently developing such a machine. Theoretical analyses have determined the absorber to be practical. This study involves the testing of a flow model of that absorber with the objective to verify loss coefficients and check for flow separation in the passages. The complete model testing process is described and the desired information determined. It is recommended that further testing of off-design point performance and separation be carried out.

DD FORM 1 NOV 68 1473 (PAGE 1)

S/N 0101-807-6811

Security Classification

A-31408

KEY WORDS	LINK A		LINK B		LINK C	
	ROLE	WT	ROLE	WT	ROLE	WT
Turbine Type Energy Absorber						
Aircraft Carrier Arresting Gear						
Model Tests						
Loss Coefficients in Flow Passages						

Thesis
M82268
c.1

143244

Morgenfeld
Model test of a turbo-type energy absorber for aircraft carrier arresting gear.